Chapter 10

Radioactivity Method

10.1. INTRODUCTION

The geophysical techniques described in previous chapters have depended on variations in the mechanical, chemical, electrical, or magnetic properties of rocks and minerals. Since about 1945 another property of certain elements has become of considerable economic importance. This property is known as *radioactivity*.

The original discovery was made by Becquerel in 1896, shortly after Röentgen had announced in 1895 the discovery of X-rays. Becquerel found that minerals containing uranium, as well as salts of uranium, emitted radiations that passed through material opaque to ordinary light, affected photographic emulsions in a manner similar to X-rays, and would ionize a gas.

The discovery of other radioactive elements soon followed. Mme. Curie, investigating minerals of uranium, extracted two new elements, polonium and radium, which were much more active than uranium. About the same time Schmidt discovered that thorium was radioactive and Debierne found the new radioactive element actinium.

Although at least 20 naturally occurring elements are now known to be radioactive, only uranium (U), thorium (Th), and an isotope of potassium (K) are of importance in exploration. One other, rubidium, is useful in determining ages of rocks, but the rest are either so rare or so weakly radioactive, or both, as to be of no significance in applied geophysics. A complete list, with characteristic radiations and other pertinent data, is given in Table 10.1.

The two elements, uranium and thorium, are important today as a source of fuel for the generation of heat and power in nuclear reactors. Large areas in all parts of the world have been surveyed on the ground and particularly by air in the search for uranium, using special detectors, which will be discussed later.

Surface work in radioactivity exploration is relatively a minor effort (see Table 1.2 for 1987 figures.) Airborne radiometric prospecting is still comparatively cheap and efficient from the point of view of detecting gamma rays (γ rays) because the intensity of a 1 MeV beam is reduced by only 50% at 100 m above surface.

Considerable airborne work was done in the late 1950s using scintillation meters with large crystals. The results were not very useful owing to the lack of discrimination in total-count measurements (§10.3.4). When the demand for uranium fell off, the technique was almost abandoned. A revival of interest in uranium in the early 1970s, plus the availability of greatly improved γ-ray spectrometers (§10.3.4), made the method more attractive. A large-scale airborne radiometric program was initiated by the Geological Survey of Canada (GSC); this provided a stimulus for ground followup by private interests in various parts of Canada (Darnley, Cameron, and Richardson, 1975; Bristow et al., 1977).

The radioactive method is relatively unimportant in comparison with other geophysical techniques. It was first used in the late thirties for stratigraphic correlation in oil well logging (§11.1.2). Radioactivity prospecting became quite popular in the period 1945–57, fell off with the decrease in demand for uranium, and was revived again in the late sixties and early seventies. This sporadic progress, however, has not affected well-logging applications of the method, where several radiometric techniques have become standard. These will be discussed in Chapter 11.

10.2. PRINCIPLES OF RADIOACTIVITY

10.2.1. Constituents of the Nucleus

(a) Introduction. Although much of the original work on emanations from radioactive substances was done by Rutherford and others nearly 80 years ago, their source – the nucleus of the atom – was not well understood at the time. We shall now consider this source and its elementary parts.

(b) Atoms. The *atom*, which is the fundamental part of all the elements, consists of a dense, small

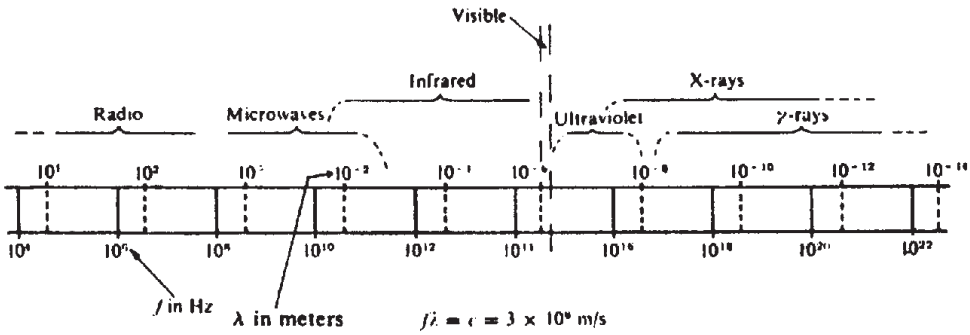

Figure 10.1. The electromagnetic spectrum showing relative frequency (wavelength) bands.

($\sim 10^{-13}$ cm in radius), positively charged nucleus surrounded by negatively charged electrons, in number equal to the nuclear charge. The arrangement is quite analogous to a solar system, with planets moving about a central sun. Because there are never more than 92 electrons and because the atomic radii are of the order 10^{-8} cm, most of the atom, like the solar system, is empty.

(c) Protons. The nucleus is composed of tightly packed *protons* and *neutrons*. The proton, carrying unit positive charge, has a mass 1.00812 on the physical scale (O = 16.0000...), the actual mass being 1.7×10^{-24} g. The number of protons in a nucleus determines the element itself. For example, the first element in the Periodic Table, hydrogen, has 1 proton, oxygen has 8, cadmium 48, and so on, up to uranium, with 92 protons.

(d) Neutrons. The other nuclear particle, the neutron, has zero charge and a slightly greater mass than the proton (1.00893). The only element lacking neutrons is common hydrogen. As we proceed through the Periodic Table, the ratio of the number of neutrons to the number of protons increases from 1 to ~ 1.5. Thus helium has 2 neutrons and 2 protons, whereas thorium contains 142 neutrons and 90 protons.

(e) Isotopes. Most elements are composed of a mixture of nuclei having different numbers of neutrons, the number of protons, of course, being the same. These are called *isotopes*, that is, forms of the same element having different atomic weights. (Practically all the mass of an element is contained in the nucleus, hence is determined by the number of protons and neutrons called the *atomic weight*). For instance, hydrogen is a mixture of two isotopes: $_1H^1$, which is a single proton (99.985% abundance), and $_1H^2$, one proton and one neutron, familiarly known as deuterium (0.015% abundance). Titanium has 5 isotopes, tin has 10, tungsten 5, lead 4, and so on.

(f) Alpha particles. Actually these are the equivalent of a helium nucleus, $2p + 2n$; the name was attached in the pioneer days of radioactivity, before the nature of the particle was understood. It has a charge +2, mass 4.00389, and is frequently a tightly bound entity within nuclei heavier than helium. It may be ejected from the nucleus during a disintegration.

(g) Electrons. The outer atomic constituent, the electron, has a charge −1 (actual charge on the electron and proton is 1.60×10^{-19} C) and mass about 1/1,840 of the proton. Although the electron does not exist as a separate entity in the nucleus, it is ejected in certain nuclear disintegrations when a neutron splits into a proton and an electron, the proton remaining in the nucleus. This transmutation results in a gain of +1 unit of charge and practically zero mass change, that is to say, the element moves up one place in the Periodic Table. Electrons ejected from the nucleus were originally called *beta* (β) particles or rays.

(h) Gamma radiation. During nuclear disintegrations, pure electromagnetic radiation representing excess energy is frequently emitted from the excited nucleus. The early name assigned, *gamma ray* (γ *ray*) is quite appropriate in this case (α and β rays are really discrete particles). Gamma rays differ from X-rays only in name, although usually the latter term is used for radiation of lower energy. The relative location of γ rays in the electromagnetic spectrum is illustrated in Figure 10.1.

10.2.2. Nuclear Disintegrations

While carrying on pioneer work in nuclear physics, Sir Ernest Rutherford investigated the radiations from naturally occurring radioactive elements and showed that they consisted of the three distinct types mentioned above: α, β, and γ rays. Each of these rays produces three different effects in varying

Table 10.1. *Naturally occurring radioactive isotopes.*

Element	Isotope	Abundance (%)	Half-life (yr)	Type of radiation	Energy (MeV)
Potassium	$_{19}K^{40}$	0.012	1.3×10^9	β, K cap	1.46
Calcium	$_{20}Ca^{48}$	0.18	$> 2 \times 10^{16}$	β	0.12
Vanadium	$_{23}V^{50}$	0.24	6×10^{15}	β, K cap	0.71, 1.59
Rubidium	$_{37}Rb^{87}$	27.8	4.7×10^{10}	β	0.27
Indium	$_{49}In^{115}$	95.72	6×10^{14}	β	0.60
Lanthanum	$_{57}La^{138}$	0.089	1.1×10^{11}	β, K cap	0.54, 0.81, 1.43
Cerium	$_{58}Ce^{142}$	11.1		α	1.5
Neodymium	$_{60}Nd^{144}$	23.8	5×10^{15}	α	1.8
Samarium	$_{62}Sm^{147}$	14.97	10^{11}	α	2.32
Samarium	$_{62}Sm^{148}$	11.2	1.2×10^{13}	α	2.14
Samarium	$_{62}Sm^{149}$	13.8	$\sim 4 \times 10^{14}$	α	1.84
Gadolinium	$_{64}Gd^{152}$	0.2	1.1×10^{14}	α	2.24
Lutecium	$_{71}Lu^{176}$	2.6	3×10^{10}	β, γ	0.088, 0.20, 0.31
Hafnium	$_{72}Hf^{174}$	0.16	2×10^{15}	α	2.5
Rhenium	$_{75}Re^{187}$	62.9	7×10^{10}	β	$\leq$ 0.008
Platinum	$_{78}Pt^{190}$	0.013	6×10^{11}	α	3.11
Platinum	$_{78}Pt^{192}$	0.78	$\sim 10^{15}$	α	2.6
Lead	$_{82}Pb^{204}$	1.48		α	
Thorium*	$_{90}Th^{232}$	100	1.39×10^{10}	α, β, γ	0.03 – 2.62
Uranium*	$_{92}U^{235}$	0.72	7.1×10^8	α, β, γ	0.02 – 0.9
Uranium*	$_{92}U^{238}$	99.3	4.5×10^9	α, β, γ	0.4 – 2.5

*Each of these undergoes a long series of disintegrations yielding lead isotopes 208, 207, 206, respectively. During these disintegrations numerous γ rays are emitted, in addition to the α- and β particles.

degrees, namely:

1. They affect photographic emulsions in much the same way as light and X-rays.
2. They ionize gas, making it electrically conducting.
3. They produce scintillations or phosphorescence in certain minerals and chemical compounds.

All three effects have been used in geophysical prospecting by the radioactivity method.

The three "rays" characteristic of natural nuclear disintegrations have very different penetrating powers. Thus, α rays are easily stopped by a sheet of paper, β rays by a few millimeters of aluminum, whereas γ radiation requires several centimeters of lead. Their equivalent range in overburden or rock is thus practically zero for the first two and not more than 50 to 75 cm of rock for γ rays.

In fact, this range is a complicated function of the energy and character of the particles or radiation and of the density or atomic number of the medium through which they pass. It is clear that the range varies with initial energy and the rate of dissipation of energy. The latter is a complex process of scattering, collision, and absorption involving the atoms of the host material and resulting in ionization along the path. Charged particles (α, β) ionize strongly, uncharged electromagnetic radiations (γ rays, X-rays) do not.

Maximum energy in natural nuclear disintegrations is generally less than 3 MeV [1 MeV = 10^6 electron-volts (eV), the energy acquired by a particle of unit charge, falling through a potential of 10^6 V.] Even in air, the range of 3 MeV α and β particles is only a few centimeters and meters, respectively. On the other hand, γ rays of this energy will travel a few hundred meters in air.

In addition to α, β, and γ emissions, there is one other type of nuclear transmutation, called *K capture* (see Table 10.1 and Fig. 10.2), which occurs in several of the natural radioelements. In this process, an electron from the innermost K orbit enters the nucleus, which then emits γ rays; as a result of the electron capture the atomic number decreases by one and a different element is created.

The equations representing transitions of element X to Y by α- and β-ray emission and electron capture are

$$_pX^{p+n} \rightarrow {}_{p-2}Y^{p+n-4} + {}_2He^4 \quad (\alpha \text{ emission})$$

$$_pX^{p+n} \rightarrow {}_{p+1}Y^{p+n} + e^- \quad (\beta \text{ emission})$$

$$_pX^{p+n} + e^- \rightarrow {}_{p-1}Y^{p+n} \quad (K \text{ capture})$$

In this nomenclature, the number of protons in elements X, Y, and He is the lower left subscript, whereas the number of protons plus neutrons (atomic weight) is given by the upper right superscript. Because the X, Y, and He symbols define the number of protons uniquely, this notation has recently been changed by entering the nuclear mass ($p + n$) at the

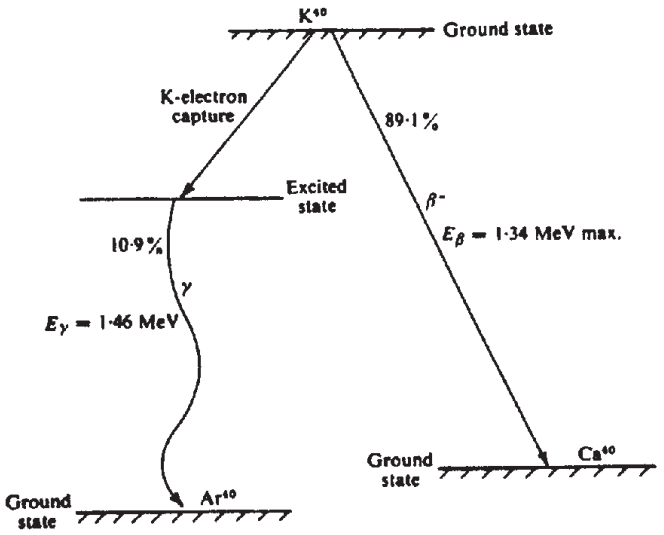

Figure 10.2. Energy-level diagram for radioactive potassium.

upper left and deleting the proton number altogether. Thus $_{37}Rb^{87}$ becomes ^{87}Rb.

10.2.3. Radioactive Decay Processes

In 1902 Rutherford and Soddy announced the theory of radioactive transformation, in which they stated that when an element emitted α or β rays, it was transmuted into a new element, the rate of disintegration being a characteristic of each radioactive nucleus. They showed that the rate of change was proportional to the number of atoms present and was not affected by physical or chemical processes in the surroundings.

Thus, for any type of radioactive atom, we have the relation

$$dN/dt = -\lambda N$$

where N is the number of atoms present at time t and λ is a decay constant that is characteristic of each element. Therefore,

$$\int_{N_0}^{N} \frac{dN}{N} = -\lambda \int_0^t dt \quad \text{or} \quad N = N_0 e^{-\lambda t} \quad (10.1)$$

where N_0 is the number of atoms at an arbitrary time $t = 0$. If $T_{1/2}$ is the time required for half of the nuclei to disintegrate, we have

$$N/N_0 = \tfrac{1}{2} = e^{-\lambda T_{1/2}}$$

or

$$\lambda = (\ln 2)/T_{1/2} = 0.693/T_{1/2} \quad (10.2)$$

Half-life values of radioactive nuclei vary enormously, from $^{212}Po \approx 10^{-7}$ s to $^{204}Pb \approx 10^{19}$ y. Obviously a short half-life goes with a vigorous rate of disintegration, whereas the lead isotope 204 is, for all practical purposes, stable – the disintegration rate is three or four nuclei per week per gram.

As mentioned earlier, only three radioactive elements, U, Th, and K are of practical significance in prospecting. The potassium is mainly a nuisance when searching for the other two; although the ^{40}K isotope is, apparently, no more plentiful than U or Th, the widespread occurrence of potassium-rich rocks and particularly the association of these with U and Th, for example, in pegmatites, creates a problem somewhat analogous to that of graphite versus metal sulfides in electrical prospecting.

As shown by Table 10.2 and Figure 10.3, there are three radioactive series for uranium and thorium, starting with $_{90}Th^{232}$, $_{92}U^{235}$ (the so-called actinium series), and $_{92}U^{238}$. All decay eventually to stable isotopes of lead, with 10, 15, and 17 intermediate radioactive stages, respectively.

It is useful to calculate the number of daughter atoms present at any time, given the number N_0 of the parent at time $t = 0$. Then the number of parent atoms left at a later time t will be $N_1 = N_0 e^{-\lambda_1 t}$, where λ_1 is its decay constant. But the rate of decay of the parent atoms, $dN_1/dt = -\lambda_1 N_1$, is just the rate of production of the daughter. At the same time the daughter atoms are disintegrating at a rate $\lambda_2 N_2$, where N_2 is the number present at time t and λ_2 is the decay constant. Hence the rate of accumulation of the daughter atoms is the difference between production and decay, or

$$dN_2/dt = \lambda_1 N_1 - \lambda_2 N_2 = \lambda_1 N_0 e^{-\lambda_1 t} - \lambda_2 N_2 \quad (10.3)$$

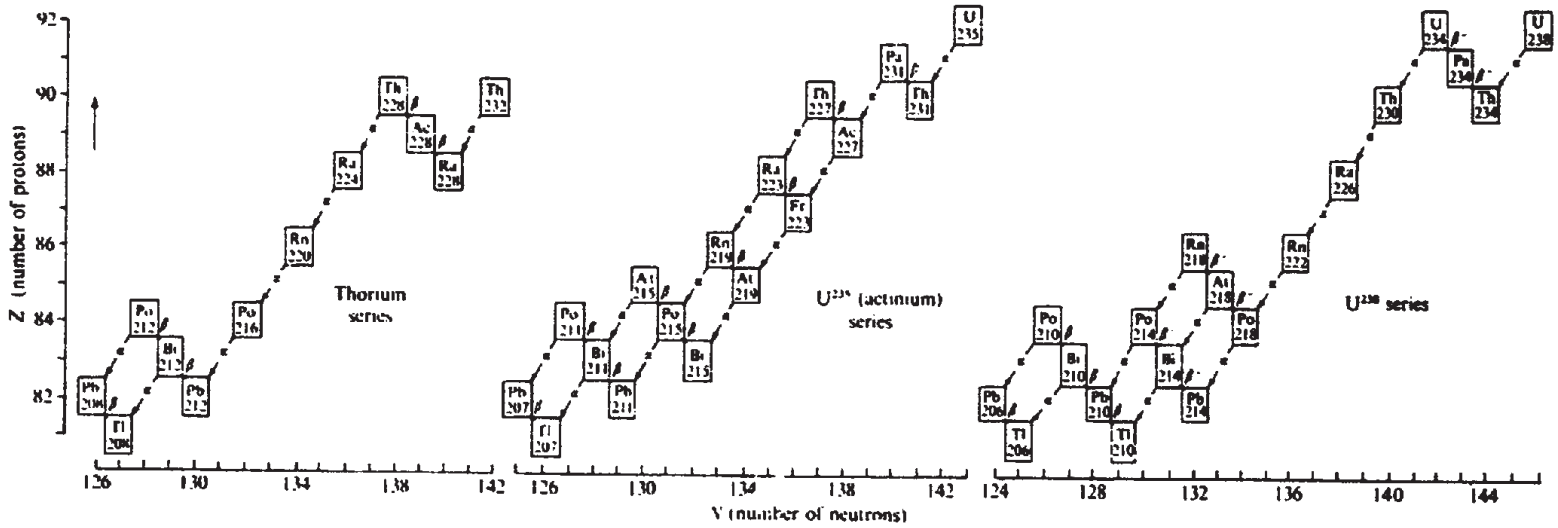

Figure 10.3. Uranium and thorium radioactive series. Schematic showing decay processes.

Table 10.2. *Natural radioactive series of thorium and uranium.*

Isotope	Half-life	Decay constant (s^{-1})	Radiation	γ-ray energies (MeV)	No. of γ-rays
Thorium series					
$_{90}Th^{232}$	1.4×10^{10} yr	1.58×10^{-18}	α, SF*, γ	0.059	
$_{88}Ra^{228}$	6.7 yr	3.3×10^{-9}	β, γ	0.03	
$_{89}Ac^{228}$	6.1 hr	3.1×10^{-4}	β, γ	0.06 – 0.97	> 10
$_{90}Th^{228}$	1.91 yr	1.15×10^{-8}	α, γ	0.085 – 0.214	5
$_{88}Ra^{224}$	3.64 day	2.2×10^{-6}	α, γ	0.24, 0.29	
$_{86}Rn^{220}$	51 s	1.3×10^{-2}	α, γ	0.54	
$_{84}Po^{216}$	0.16 s	4.3	α		
$_{82}Pb^{212}$	10.6 hr	1.8×10^{-5}	β, γ	0.11 – 0.41	5
$_{83}Bi^{212}$	60.6 min	1.9×10^{-4}	β, α, γ	0.04 – 2.2	> 10
$_{84}Po^{212}$	0.3×10^{-6} s	2.3×10^{6}	α		
$_{81}Tl^{208}$	3.1 min	3.7×10^{-3}	β, γ	0.28 – 2.62	5
$_{82}Pb^{208}$	Stable				
Actinium Series					
$_{92}U^{235}$	7.1×10^{8} yr	3.1×10^{-17}	α, SF*, γ	0.07 – 0.38	10
$_{90}Th^{231}$	25.6 hr	7.4×10^{-6}	β, γ	0.08 – 0.31	> 10
$_{91}Pa^{231}$	3.4×10^{4} yr	6.5×10^{-13}	α, γ	0.29 – 0.36	> 10
$_{89}Ac^{227}$	21.6 yr	10^{-9}	β, α, γ	0.09 – 0.19	9
$_{90}Th^{227}$	18.2 day	4.35×10^{-7}	α, γ	0.05 – 0.33	> 10
$_{87}Fr^{223}$	22 min	5.2×10^{-4}	β, α, γ	0.05 – 0.31	4
$_{88}Ra^{223}$	11.7 day	6.76×10^{-7}	α, γ	0.03 – 0.45	> 10
$_{86}Rn^{219}$	4 s	0.17	α, γ	0.27, 0.4	
$_{85}At^{219}$	54 s	1.28×10^{-2}	α, β		
$_{84}Po^{215}$	1.8×10^{-3} s	3.8×10^{2}	α, β		
$_{85}At^{215}$	10^{-4} s	6.9×10^{3}	α		
$_{83}Bi^{215}$	8 min	1.44×10^{-3}	β		
$_{83}Bi^{211}$	2.15 min	5.35×10^{-3}	α, β, γ	0.35	
$_{84}Po^{211}$	0.52 s	1.32	α, γ	0.56, 0.88	
$_{82}Pb^{211}$	36 min	3.2×10^{-4}	β, γ	0.065 – 0.83	4
$_{81}Tl^{207}$	4.8 min	2.4×10^{-3}	β, γ	0.89	
$_{82}Pb^{207}$	Stable				
Uranium Series					
$_{92}U^{238}$	4.51×10^{9} yr	4.9×10^{-18}	α, SF*, γ	0.048	
$_{90}Th^{234}$	24.1 day	3.3×10^{-7}	β, γ	0.03 – 0.09	3
$_{91}Pa^{234}$	6.7 hr	2.84×10^{-5}	β, γ	0.044 – 1.85	> 10
$_{92}U^{234}$	2.48×10^{5} yr	8.9×10^{-14}	α, SF*, γ	0.053, 0.118	
$_{90}Th^{230}$	8×10^{4} yr	2.75×10^{-10}	α, γ	0.068 – 0.25	7
$_{88}Ra^{226}$	1622 yr	1.35×10^{-11}	α, γ	0.19 – 0.64	4
$_{86}Rn^{222}$	3.82 day	2.07×10^{-6}	α, γ	0.51	
$_{84}Po^{218}$	3.05 min	3.8×10^{-3}	α, β		
$_{85}At^{218}$	1.35 s	0.51	α		
$_{86}Rn^{218}$	0.03 s	23.1	α	0.61	
$_{83}Bi^{214}$	19.7 min	5.85×10^{-4}	β, α, γ	0.45 – 2.43	> 10
$_{84}Po^{214}$	1.64×10^{-4} s	4.2×10^{3}	α		
$_{82}Pb^{214}$	26.8 min	4.3×10^{-4}	β, γ	0.05 – 0.35	> 10
$_{82}Pb^{210}$	21 yr	1.05×10^{-9}	β, γ	0.047	
$_{83}Bi^{210}$	5 day	1.58×10^{-6}	β		
$_{84}Po^{210}$	138.4 day	5.7×10^{-8}	α, γ	0.79	
$_{81}Tl^{210}$	1.3 min	8.85×10^{-3}	β, γ	0.3, 0.78, 1.1	
$_{81}Tl^{206}$	4.2 min	2.75×10^{-3}	β		
$_{82}Pb^{206}$	Stable				

SF* = spontaneous fission.

We can solve this equation by assuming $N_2 = Ae^{-\lambda_1 t} + Be^{-\lambda_2 t}$, with the condition that, when $t = 0$, $N_2 = 0$. The result is

$$N_2 = \frac{\lambda_1 N_0}{\lambda_2 - \lambda_1}(e^{-\lambda_1 t} - e^{-\lambda_2 t}) \quad (10.4a)$$

This calculation can be carried on for successive members of the series. The number of atoms of the nth product produced after time t is given by

$$N_n = C_1 e^{-\lambda_1 t} + C_2 e^{-\lambda_2 t} + \cdots + C_n e^{-\lambda_n t} \quad (10.4b)$$

Table 10.3. *Emission of γ rays by U and Th series and by K.*

Energy (MeV)	Uranium series (Phot/s g)	%U	Thorium series (Phot/s g)	%Th	Potassium (Phot/s g)	%K
0.2 – 0.5	9.4×10^3	36	3.9×10^3	34		
0.5 – 1.0	8.0×10^3	31	5.5×10^3	47		
1.0 – 1.5	4.3×10^3	17	0.4×10^3	3	3.4	100
1.5 – 2.0	3.2×10^3	12	0.3×10^3	3		
2.0 – 2.5	1.1×10^3	4				
2.5 – 3.0			1.5×10^3	13		
Total	2.6×10^4	100	1.2×10^4	100	3.4	100

where

$$C_1 = \frac{\lambda_1\lambda_2 \cdots \lambda_{n-1}N_0}{(\lambda_2 - \lambda_1)(\lambda_3 - \lambda_1)\cdots(\lambda_n - \lambda_1)} = KN_0/\delta_1$$

$$C_2 = \frac{\lambda_1\lambda_2 \cdots \lambda_{n-1}N_0}{(\lambda_1 - \lambda_2)(\lambda_3 - \lambda_2)\cdots(\lambda_n - \lambda_2)} = KN_0/\delta_2$$

$$\vdots$$

$$C_n = \frac{\lambda_1\lambda_2 \cdots \lambda_{n-1}N_0}{(\lambda_1 - \lambda_n)(\lambda_2 - \lambda_n)\cdots(\lambda_{n-1} - \lambda_n)} = KN_0/\delta_n \qquad (10.4c)$$

where

$$K = \lambda_1\lambda_2 \cdots \lambda_{n-1},$$

and

$$\delta_i = (\lambda_1 - \lambda_i)(\lambda_2 - \lambda_i)\cdots(\lambda_n - \lambda_i).$$

10.2.4. Radioactive Equilibrium

From Equation (10.3) it follows that when a radioactive series is in equilibrium, we have

$$\lambda_1 N_1 = \lambda_2 N_2 = \lambda_3 N_3 = \cdots \lambda_n N_n. \quad (10.5)$$

That is to say, at equilibrium the number of daughter atoms disintegrating per second is the same as the number being created by disintegrations of the parent.

The state of radioactive equilibrium merits further explanation. Consider radium and radon, the successive intermediate products in the ^{235}U series (see $_{88}Ra^{223}$ and $_{86}Rn^{219}$, Table 10.2 and Fig. 10.3). Here the daughter product decays about 10^5 times faster than its parent. If we start with a sample of pure radium, we find that its decay rate is practically constant for the first day or two, because the half-life is about 12 days. During the same interval the supply of radon atoms is building up at the same rate, although the radon is decaying considerably faster than the radium. From Equations (10.1) and (10.4a) we can get the ratio of the number of atoms of parent to daughter at any time

$$\frac{N_2}{N_1} = \frac{\lambda_1}{\lambda_2 - \lambda_1}\{1 - e^{(\lambda_1 - \lambda_2)t}\}.$$

When equilibrium has been reached, the rates of decay of parent and daughter are the same, that is, $N_2/N_1 = \lambda_1/\lambda_2$. Thus we have

$$\frac{\lambda_1}{\lambda_2} = \frac{\lambda_1}{\lambda_2 - \lambda_1}\{1 - e^{(\lambda_1 - \lambda_2)t_{eq}}\}$$

or

$$e^{(\lambda_1 - \lambda_2)t_{eq}} = \frac{\lambda_1}{\lambda_2}$$

hence,

$$t_{eq} = \left(\frac{1}{\lambda_1 - \lambda_2}\right)\ln\left(\frac{\lambda_1}{\lambda_2}\right) \qquad (10.6a)$$

For this example the value of t_{eq} is about 1 min, after which the two will be in equilibrium, as long as the radium holds out.

In the case of a series with n products, the time to reach equilibrium can be found from Equation (10.4b). It is

$$\frac{N_n}{N_1} = K\left\{\frac{1}{\delta_1} + \frac{e^{(\lambda_1 - \lambda_2)t_{eq}}}{\delta_2} + \frac{e^{(\lambda_1 - \lambda_3)t_{eq}}}{\delta_3} + \cdots + \frac{e^{(\lambda_1 - \lambda_n)t_{eq}}}{\delta_n}\right\} = \frac{\lambda_1}{\lambda_n} \quad (10.6b)$$

where K and δ were defined in Equation (10.4c).

For thorium this time interval is less than 100 yr and for the two uranium chains, of the order 10^6 yr. Measurement of series products, in which the equilibrium situation is significant, will be discussed later; under these conditions it is possible to determine the amount of a parent product in a sample by measuring the amount of one of the succeeding members.

Table 10.2 and Figure 10.3 show the three radioactive series in detail, with the principal radiation accompanying each disintegration. There is in addition a wide spectrum of γ rays accompanying both α

Table 10.4. *Radioactive minerals.*

Potassium	Mineral	(i) Orthoclase and microline feldspars [$KAlSi_3O_8$]
		(ii) Muscovite [$H_2KAl(SiO_4)_3$]
		(iii) Alunite [$K_2Al_6(OH)_{12}SO_4$]
		(iv) Sylvite, carnallite [KCl, $MgCl_2 . 6H_2O$]
	Occurrence	(i) Main constituents in acid igneous rocks and pegmatites
		(ii) Same
		(iii) Alteration in acid volcanics
		(iv) Saline deposits in sediments
Thorium	Mineral	(i) Monazite [ThO_2 + rare earth phosphate]
		(ii) Thorianite [(Th, U)O_2]
		(iii) Thorite, uranothorite [$ThSiO_4$ + U]
	Occurrence	(i) Granites, pegmatites, gneiss
		(ii) Granites, pegmatites, placers
		(iii) Same
Uranium	Mineral	(i) Uraninite [oxide of U, Pb, Ra + Th, rare earths]
		(ii) Carnotite [$K_2O.2UO_3.V_2O_5.2H_2O$]
		(iii) Gummite [uraninite alterations]
	Occurrence	(i) Granites, pegmatites, and with vein deposits of Ag, Pb, Cu, etc.
		(ii) Sandstones
		(iii) Associated with uraninite

Table 10.5. *Background radioactivity in rocks and waters.*

Rock	Ci/g ($\times 10^{-12}$)	K (ppm)	Th (ppm)	U (ppm)	Water (radium)	Ci/g ($\times 10^{-12}$)
Hornblende	1.2				Saratoga, NY	0.01 – 0.1
Granite	0.7 – 4.8	35,000	15	4	Bath, England	0.14
Basalts	0.5	9,000	2	0.6	Carlsbad, Czech.	0.04 – 0.1
Olivine	0.33				St Lawrence River	0.00025
Ultramafics		10	0.2	0.05	Valdemorillo, Spain	0.02
Marble	1.9				Aix-les-Bains, France	0.002
Quartzite	5.0				Manitou, CO	0.003
Sandstone	2 – 4				Hot Springs, AR	0.0009
Slates	3 – 8				Atlantic Ocean	0.014 – 0.034
Dolomites	8				Indian Ocean	0.007
Chalk	0.4					
Chondrites		850	0.08	0.02		
Iron meteor.			0.015	0.04		

and β emission, some of which are included in the table; also, Table 10.3 gives γ-ray emissions in units of photons per second per gram for various energy windows. The thorium series has an isolated γ ray from ^{208}Tl at 2.62 MeV; the uranium series do not produce such distinctive radiations, although the 1.76 MeV γ ray from ^{214}Bi is reasonably so.

10.2.5. Units

The unit used for measuring the activity of a radioactive specimen is the *curie* (Ci) named for the discoverer of radium, Mme. Curie. It is the activity, that results in 3.7×10^{10} disintegrations per second, this being the number of α particles emitted by 1 g of pure radium, ^{226}Ra, in 1 s.

Because γ rays are similar in nature to X-rays, the strength or intensity of gamma radiation (as well as α and β particles) is also measured in the X-ray unit, called the *röentgen*. This is the quantity of radiation that will produce one electrostatic unit of charge (2.08×10^9 ion pairs) per cubic centimeter in air at 0°C and 760 Torr (NTP). Subunits are the milliröentgen (mR) and microröentgen (μR). This is the unit used in defining maximum dosage permissible to humans exposed to radioactivity, about 300 mR/week.

Some field instruments indicate radioactivity as counts per minute, generally marked on the scale of a microammeter in an integrating circuit that adds up pulses to measure total intensity. None of these units takes into account the energy of the radiation.

10.2.6. Radioactivity of Rocks and Minerals

Some of the common radioactive minerals of Th and U are listed in Table 10.4. The potassium minerals, as mentioned previously, are very widespread. Large deposits of monazite are found in Brazil, India, and South Africa. Thorite and uraninite (pitchblende) occur particularly in Canada (Great Bear Lake, northern Saskatchewan; Blind River, Ontario), in Zaïre, Central Europe (Saxony and Czechoslovakia), Malagasy, and so forth.

Trace quantities of radioactive material are found in all rocks. Along with minute amounts of cosmic radiation always present in the air, these trace amounts produce a continuous background reading, which may vary from place to place by as much as a factor of 5. Table 10.5 gives the activity and/or trace amounts of radioactivity of a number of typical rocks, as well as the amount of radium in waters.

In general the activity in sedimentary rocks and metamorphosed sediments is higher than that in igneous and other metamorphic types, with the exception of potassium-rich granites.

10.2.7. Age Determination Using Radioisotopes

Determining the age of rocks is often an important factor in developing an overall geological picture of an area and thus is indirectly relevant to applied geophysics. Isotope ratios that are useful for geological age dating include the natural disintegration reactions $^{87}Sr/^{87}Rb$, $^{40}Ar/^{40}K$, $^{146}Sm/^{147}Nd$, $^{14}C/^{12}C$, various Pb/U and Pb/Th ratios, and others.

For the decay process $^{87}Rb \rightarrow {}^{87}Sr + \beta$, taking the initial number of ^{87}Rb atoms as N_0 and assuming that no ^{87}Sr atoms were present initially, Equation (10.1) shows that the numbers of rubidium and strontium atoms now present, N_{Rb} and N_{Sr}, are

$$N_{Rb} = N_0 e^{-\lambda t} \qquad N_{Sr} = N_0(1 - e^{-\lambda t})$$

so that

$$N_{Sr}/N_{Rb} = (1 - e^{-\lambda t})/e^{-\lambda t} = (e^{\lambda t} - 1)$$

Thus, knowing the decay constant λ, the time t can be determined by measuring the ratio of ^{87}Sr to ^{87}Rb. Because the half-life is 4.9×10^{10} years, the Sr/Rb method is useful in determining the age of Precambrian rocks. An advantage of the Sr/Rb method is that all products are solids and therefore unlikely to have been lost. Minerals suitable for analysis include mica, feldspar, granite, and gneiss.

The half-life of ^{40}K is about 1.4×10^9 years; thus the K/Ar method is useful in determining ages from about 50 thousand years to about 3.5 billion years. The reaction is complicated because ^{40}K disintegrates in two ways: (i) capture of an electron from the innermost shell (K capture): $^{40}K + e \rightarrow {}^{40}Ar$; (ii) beta emission: $^{40}K \rightarrow {}^{40}Ca + \beta$. Each reaction has its characteristic decay constant, so that the ratio of the rates of decay is constant; therefore the existence of the dual decay modes does not interfere with the use of ^{40}K for dating. However, ^{40}Ca also occurs naturally and this makes the second mode unsuitable for dating. Using the first mode, the ^{40}Ar can be obtained by melting the specimen. An alternative method is to place the sample in the neutron flux of a nuclear reactor where stable ^{39}K (which has a fixed abundance ratio relative to ^{40}K) undergoes the reaction $^{39}K + e \rightarrow {}^{39}Ar$; the age can then be determined from the ratio $^{40}Ar/^{39}Ar$, this ratio being found by mass spectrographic analysis. This method yields high accuracy because mass spectrographic ratios can be determined to better than 0.01%.

Argon diffuses rapidly above 300°C, hence ^{40}K measurements determine the age since the temperature of the rock dropped below about 200°C. ^{40}Ar is also present in the atmosphere and this sometimes results in contamination; ^{40}Ar (presumably coming from trapped magmatic gases) is sometimes a contaminant in ocean-floor basalts. Minerals suitable for analysis by the ^{40}K method include mica, hornblende, and plagioclase feldspars.

Several isotope rations can be measured for the disintegration series $^{238}U \rightarrow {}^{206}Pb$, $^{235}U \rightarrow {}^{207}Pb$, and $^{232}Th \rightarrow {}^{208}Pb$. Having several different ratios to measure permits confirmation of determinations. Ratios sometimes measured include $^{207}Pb/U$, $^{206}Pb/U$, $^{208}Pb/Th$, $^{207}Pb/^{206}Pb$ (since the ratio of $^{235}U/^{238}U$ is fixed). Zircon is especially suitable for such analyses.

^{14}C has a half-life of 5,730 years and disintegrates according to the equation $^{14}C \rightarrow {}^{14}N$, ^{14}N then disintegrating to give stable ^{12}C finally. The reaction is used to date events during the last 30,000 years or so. The ^{14}C is produced in the upper atmosphere by cosmic-ray bombardment of ^{14}N. The carbon subsequently becomes incorporated in plants, animals, or other materials; the ratio of ^{14}C to ^{12}C (or other carbon isotopes) gives the time elapsed since the plant or animal was alive.

The ^{18}O to ^{16}O ratio in ocean waters changes during cool continental glacial periods and hence the ^{18}O to ^{16}O ratio is an indicator of paleo-temperatures. Although not useful for age determinations, the ratio of oxygen isotopes is a useful tool in the study of depositional temperature changes that are associated with the low-stand sea-level patterns sometimes seen in seismic data.

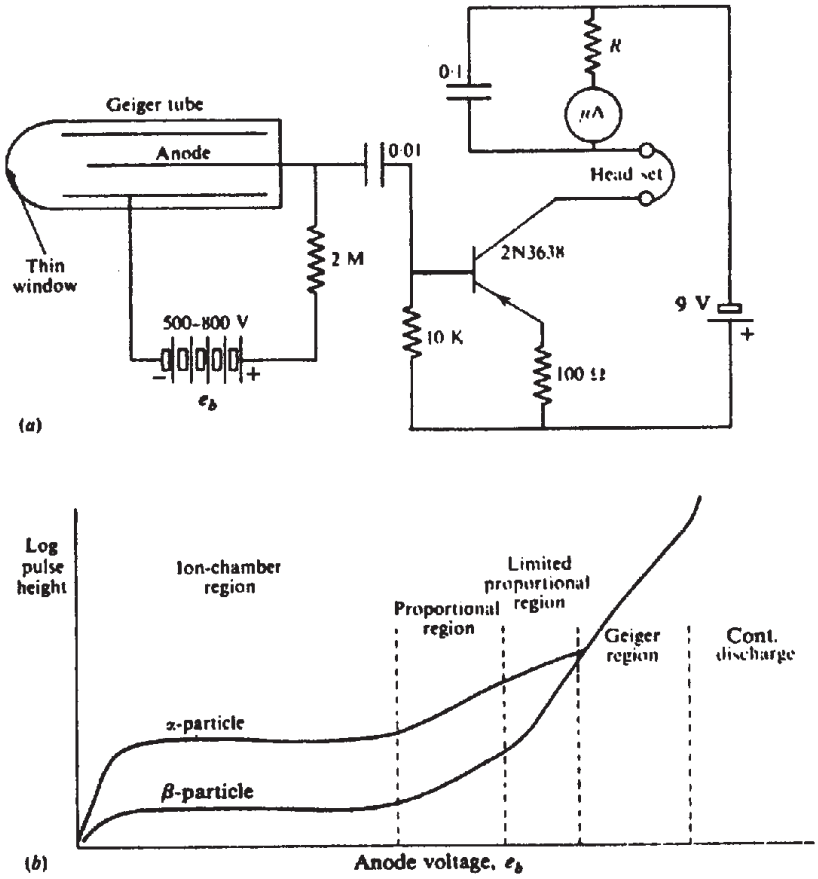

Figure 10.4. Geiger-Müller counter. (a) Simplified counter circuit. (b) Geiger-tube characteristics as a function of anode voltage.

The foregoing age determinations all assume that the system is closed, that is, no daughter isotopes were present at the beginning and none escaped from the system up to the time of measurement. If some daughter isotopes were lost in some manner, for example, by reheating above a critical temperature which resulted in the loss of the daughter isotopes, the radioisotope clock is "reset" and the abundance ratios give the time elapsed since the loss occurred. Zircon seems to be especially resistant to resetting so that analysis of zircons from granite overgrown rims using an ion microprobe gives ages different from those of zircons in the core (which presumably came from the original source of the granite). Thus, it is possible at times to date processes as well as rock samples.

10.3. INSTRUMENTS

10.3.1. Introduction

Various devices have been used for the detection of radioactivity. One of the earliest was the *ionization chamber*. At present there are two principal instruments, the *Geiger counter* and the *scintillation meter*, plus the *pulse-height analyzer* or *γ-ray spectrometer*, which is an extension of the scintillation meter. Both these detectors also were used very early in the course of radioactivity study. In their present prospecting form they are adaptations of laboratory instruments developed in the period 1944–50.

The heart of the radioactive detector is a device that will respond efficiently to β and γ radiation (α particles have such short ranges that they need not be considered generally). As noted previously, natural β rays also have a short range, even in air; hence a β detector is effective only within a few meters of the source. Consequently gamma-radiation detection is most desirable.

10.3.2. Geiger–Müller Counter

This is a very simple device that responds primarily to β radiation. Consequently it can be used only in ground traversing. A diagram showing the essential parts is given in Figure 10.4a. Like the ionization chamber, the detector is a thin-walled cylindrical tube, often with a very thin (≤ 0.025 mm) mica window in the end, to permit the passage of β particles.

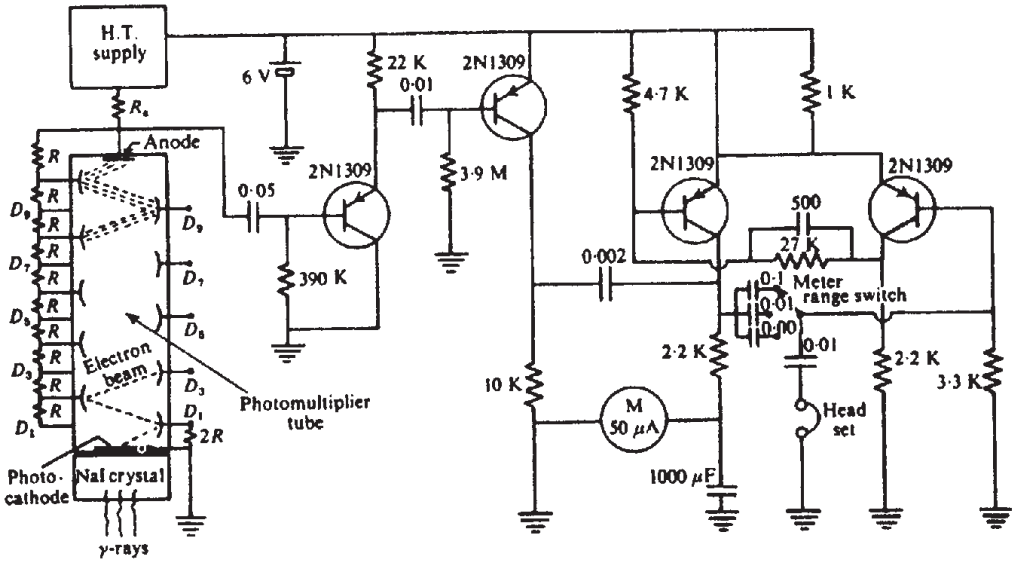

Figure 10.5. Scintillation-meter schematic.

The tube contains an axial anode wire with a coaxial cathode cylinder and is filled to a pressure of about 0.1 atm with an inert gas, such as argon, plus a trace of alcohol, methane, water vapor, or a combination of these. This gas mixture produces a quenching action. A dry cell or other low-current source supplies several hundred volts across the diode, as shown in the diagram.

Radiation entering the tube ionizes gas atoms and the positive ions and electrons are accelerated by the high voltage to the cathode and anode, respectively. These charges also ionize other gas atoms en route. The ionization is cumulative and the original ray produces a discharge pulse across the anode resistor, which is amplified in the transistor stage to produce a click in the headphones. Figure 10.4a also shows a simple integrating circuit in series with the headset. Successive pulses charge up the condenser which then leaks off slowly through the high resistance R, in series with the microammeter. The meter registers a current proportional to the integral of the charge entering the condenser.

The purpose of the quenching agent is to suppress secondary electron emission from the cathode, caused by positive ion bombardment. This effect tends to prolong the discharge. Fast quenching of the discharge allows the tube to return quickly to the nonconducting state and hence respond to succeeding rays entering the chamber shortly after the first. Although even in a good tube the clean-up time is still appreciable, it can be reduced to less than 100 μs with a suitable quenching gas mixture.

The electronic section of Figure 10.4a is oversimplified. Normally the Geiger tube pulse drives a multivibrator circuit which shapes the pulses as well as amplifying them.

Figure 10.4b shows the characteristics of the Geiger tube as a function of anode voltage. Normally the voltage is kept within the plateau (ion-chamber) region of the curve, where pulse height is independent of the voltage, thus reducing the effect of variations in battery voltage.

The prospecting Geiger counter has the virtue of being simple and cheap. However, it has little else to recommend it. It must be held close to the outcrop to detect β rays (because it is an extremely inefficient detector of γ rays, which are weak ionizers and tend to pass right through the tube without being registered). Lead fins have been mounted on the outside of the tube to degrade and convert the γ rays to β rays; however, this has not improved the efficiency enough to make the instrument competitive with the scintillation meter. Thus the Geiger counter remains a tool of limited application.

10.3.3. Scintillation Meter

(a) General. The counting of scintillations produced by radiation bombardment of a zinc sulfide screen was one of the earliest methods of detection. Other materials that have been used for this purpose include anthracene, stilbene, and scheelite. One of the best scintillation detectors is made by growing natural crystals of sodium iodide (NaI), treated with thallium (Tl). The NaI is transparent to its own fluorescent emission and all faces but one are coated with light reflecting material. If the crystal is large enough, its conversion efficiency for natural (< 3

MeV) γ rays is practically 100%. A portable device of this type became possible following the development of the photomultiplier tube.

(b) Gamma-ray interactions. As mentioned briefly in Section 10.2.2, the dissipation of energy as radiation passes through matter is a complex process. To explain the operation of the scintillation meter, it is necessary to discuss the sequence of events in which the radiation is absorbed. The interaction of γ radiation with matter takes place by the following processes (see also §11.8.1c).

(i) The *photoelectric effect*, in which the γ ray loses all of its energy to a bound atomic electron, part of the energy being used to overcome its binding to the atom, the remainder appearing as kinetic energy of the electron. This effect predominates at low energy ($\leq$ 200 keV) although it also varies greatly with the atomic number of the absorbing material.

(ii) *Compton scattering* by atomic electrons, in which the γ ray is deflected in its path. When the γ-ray energy is much larger than the electron binding energy (which varies from $\sim 10^5$ eV for innermost K electrons of heavy elements to a few electron volts in light elements), the scattering takes place as though the electrons were unbound and at rest. This is the dominant interaction at intermediate energies (100 keV to 2 MeV), and the effect of atomic number is not so pronounced.

(iii) *Pair production*, in which the γ ray is annihilated near a nucleus or electron while creating an electron–positron (positive electron) pair. The energy required for this process must be greater than the rest energy (energy equivalent to the mass) of the pair; any excess appears as kinetic energy of the electron and positron. Because the electron rest energy is 0.51 MeV, pair production cannot take place unless the γ-ray energy originally was larger than 1.02 MeV. Hence it is essentially a high-energy phenomenon.

Of these three modes of interaction, the first is most desirable for γ-ray spectroscopy (see next section), because the original radiation is converted to a light photon, giving up all its energy in the process. For the ordinary scintillation meter, however, the only requirement is that the input γ rays be eventually converted to light, regardless of the mode of absorption.

(c) Description of scintillation meter. A schematic of the scintillation meter is shown in Figure 10.5. Light generated in the NaI crystal by γ conversion falls on the semitransparent photocathode of the photomultiplier tube, causing electron emission. The crystal and multiplier tube are mounted as a single unit in a light-tight cylindrical can, the crystal face being in contact with the photocathode end.

The electrons emitted from the photocathode are accelerated toward the first electrode, D_1, operating at $\sim$ 150 V positive with respect to the grounded cathode. The intermediate electrodes, D_1 to D_{10}, called dynodes and usually $\sim$ 10 in number, provide electron multiplication by secondary emission from surfaces coated with low work-function material, for example, Cs_3Sb, the chain being so mounted that the electrons must proceed from D_1 to D_2, and so forth, then finally to the anode. With a gain factor of $\sim$ 4 per stage, the total current amplification is roughly 10^6. This produces a current pulse of about 0.5 μA through the anode resistor, R_a, and the resulting voltage pulse of some 20 mV is amplified and integrated as in the Geiger counter circuit.

The great advantage of this instrument is in the efficiency of γ-ray detection. It will also detect β rays. The price is about 10 times that of a Geiger counter and the size and weight are somewhat greater than the Geiger. It can be used in completely portable form (frequently with detachable crystal-multiplier head for entering a confined space), or as a semiportable unit in a car or aircraft. The airborne instrument is much more elaborate. Portable sets usually have crystals 40 to 75 mm diameter, 25 to 75 mm thick, with a multiplier photocathode to match the diameter. The earlier airborne versions used several crystals about 100 mm thick and 200 to 250 mm diameter, with a group of photomultipliers (three to seven) on each crystal; this was necessary to maximize the light collection, because the photocathode diameter was limited. Such an arrangement required manipulation of many gain adjustments to optimize the overall resolution. More recently arrays of four to six prismatic crystals 400 mm long and 100 × 100 mm cross section with a single multiplier mounted on one end of each have resulted in a compact packaged-slab geometry and reduced the equalization time. Airborne units are equipped with analog and digital readouts.

Further improvements in scintillation meter detection may result from using (i) relatively huge organic plastics as scintillators, (ii) germanium solid-state detectors, (iii) combination NaI-CsI crystals, and (iv) silicon-diode "one-shot" photomultiplier tubes.

10.3.4. Gamma-Ray Spectrometer

A logical extension of the scintillometer is a spectrometer that separates characteristic γ rays of ^{40}K, U, and Th for identification of the source. Such instruments are widely used in airborne surveys and a couple of portable units are also available.

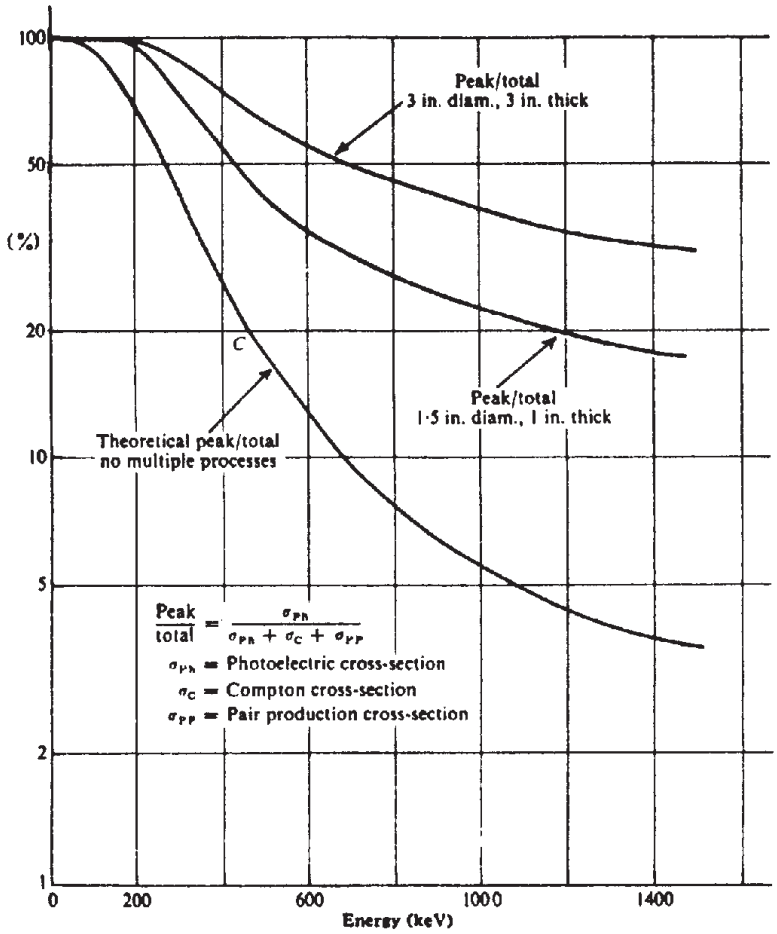

Figure 10.6. γ-ray absorption efficiency in NaI crystals.

Spectrometers of this type, known as *pulse-height analyzers* or "kick sorters," have been used for γ-ray analysis in nuclear physics laboratories for some 40 years. They make use of the fact that the intensity of the light pulse, and hence the amplitude of the voltage pulse from the multiplier, is proportional to the original γ-ray energy. Actually this is only partially true, due to the complex process of γ-ray absorption, and further explanation is necessary.

When the γ-ray loses all of its initial energy at once by photoconversion, the preceding statement is entirely correct. Even if it is first degraded by scattering and/or pair production, resulting eventually in photoelectrons of lower energy, these will still add up to a pulse of the same amplitude, *provided* the γ ray does not escape from the crystal, that is, it is completely absorbed. This is true because all the processes occur essentially simultaneously (because γ rays, being electromagnetic radiation, travel with the velocity of light). However, if the beam of γ rays entering the crystal were monochromatic, of energy E, and some rays escape with lower energy e, there is a contribution to the pulse-height spectrum corresponding to $E - e$.

Figure 10.6 illustrates the efficiency of NaI crystals in converting the γ rays into pulses of maximum amplitude by multiple processes. A theoretical curve C shows the ratio of cross section (effectively absorption) by photoconversion only, to total cross section, that is, all three conversion processes, for comparison. For energies between 1.5 MeV and 100 keV (below which the photoelectric effect predominates) the larger crystal is on average 35% more efficient, whereas the smaller loses an increasingly larger fraction of γ rays by scattering out of the crystal.

To obtain 100% efficiency in converting the γ rays, it would be necessary to mount the radioactive source, as a minute grain, inside the crystal, and in fact this is done in laboratory installations. In these circumstances – and provided the crystal is large enough – all the γ rays would be absorbed in the crystal and the original γ-ray spectrum of the source would be quite faithfully reproduced as a pulse-voltage spectrum in the analyzer. In a field measurement, however, the situation is more complicated. Some γ rays lose energy by scattering in escaping from the source and also during passage through the

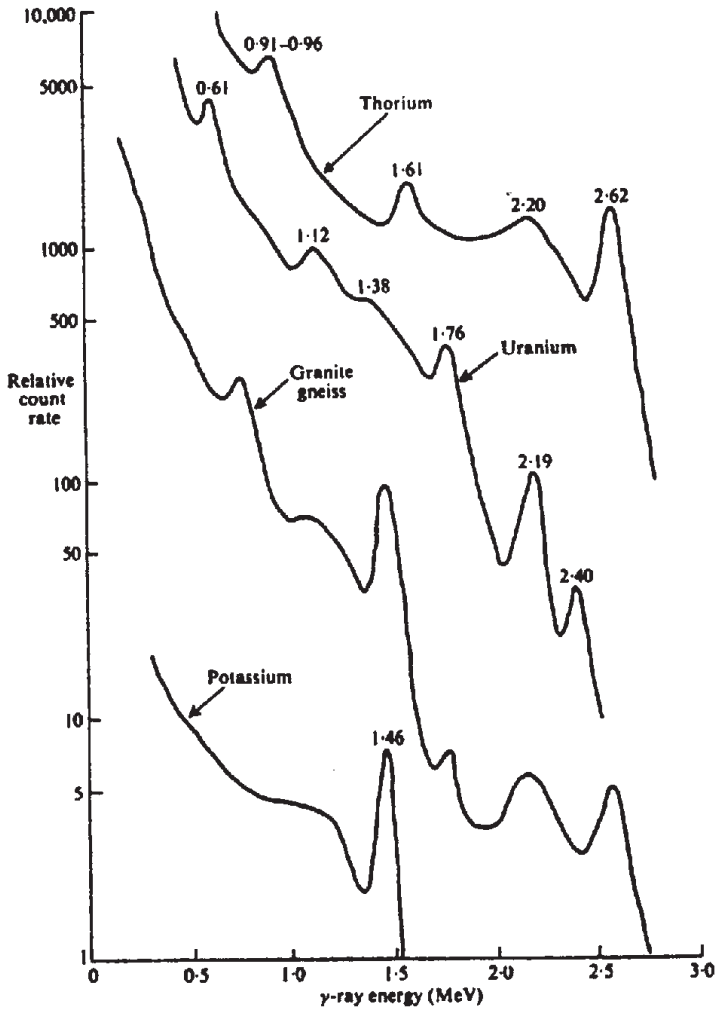

Figure 10.7. γ-ray spectra of K, U, and Th samples and granite-gneiss outcrop.

air to the crystal. This, coupled with the fact that the U and Th series emit numerous γ rays over a wide energy range, results in a complex pulse-height spectrum, as shown in Figure 10.7. All four curves have characteristic peaks and, in addition, an increasing continuum at low energies, due to Compton scattering. The pure potassium sample produces a relatively simple curve, having only the ^{40}K peak at 1.46 MeV. Thorium is characterized by the strong 2.62 MeV peak of ^{208}Tl. The uranium spectrum is most complex, although the peak at 1.76 MeV is reasonably distinctive. Potassium and thorium are clearly evident in the granite gneiss, as well as a smaller fraction of uranium.

A prospecting γ-ray spectrograph, then, should be capable of isolating the K, U, and Th peaks at 1.46, 1.76, and 2.62 MeV. This is accomplished by replacing the integrator–counter circuit in the scintillation meter with three electronic circuits to select the appropriate pulse heights that correspond to the preceding γ-ray energies. Considering channel 2 in Figure 10.8a, the detail diagram at the upper right of the figure shows that the channel is actually two parallel channels. The discriminator 2A is biased so that it gives an output pulse only for γ rays with energy greater than 1.36 MeV, whereas discriminator 2B responds only to γ rays with energy in excess of 1.56 MeV. Thus neither discriminator registers γ rays whose energies are less than 1.36 MeV, whereas for values greater than 1.56 MeV the anticoincidence circuit adds the two outputs out of phase to give zero output as well.

The other two channels operate in the same manner for 1.76 and 2.26 MeV. Generally the channel centers and widths are adjustable. Clearly the window must be wide enough to accommodate the finite width of the peaks in Figure 10.7, but not so wide that the flanks of adjacent peaks may be accepted as well.

The pulses are counted and integrated separately and, in the airborne instrument, applied to a three-channel recorder. Because the radioactive sources

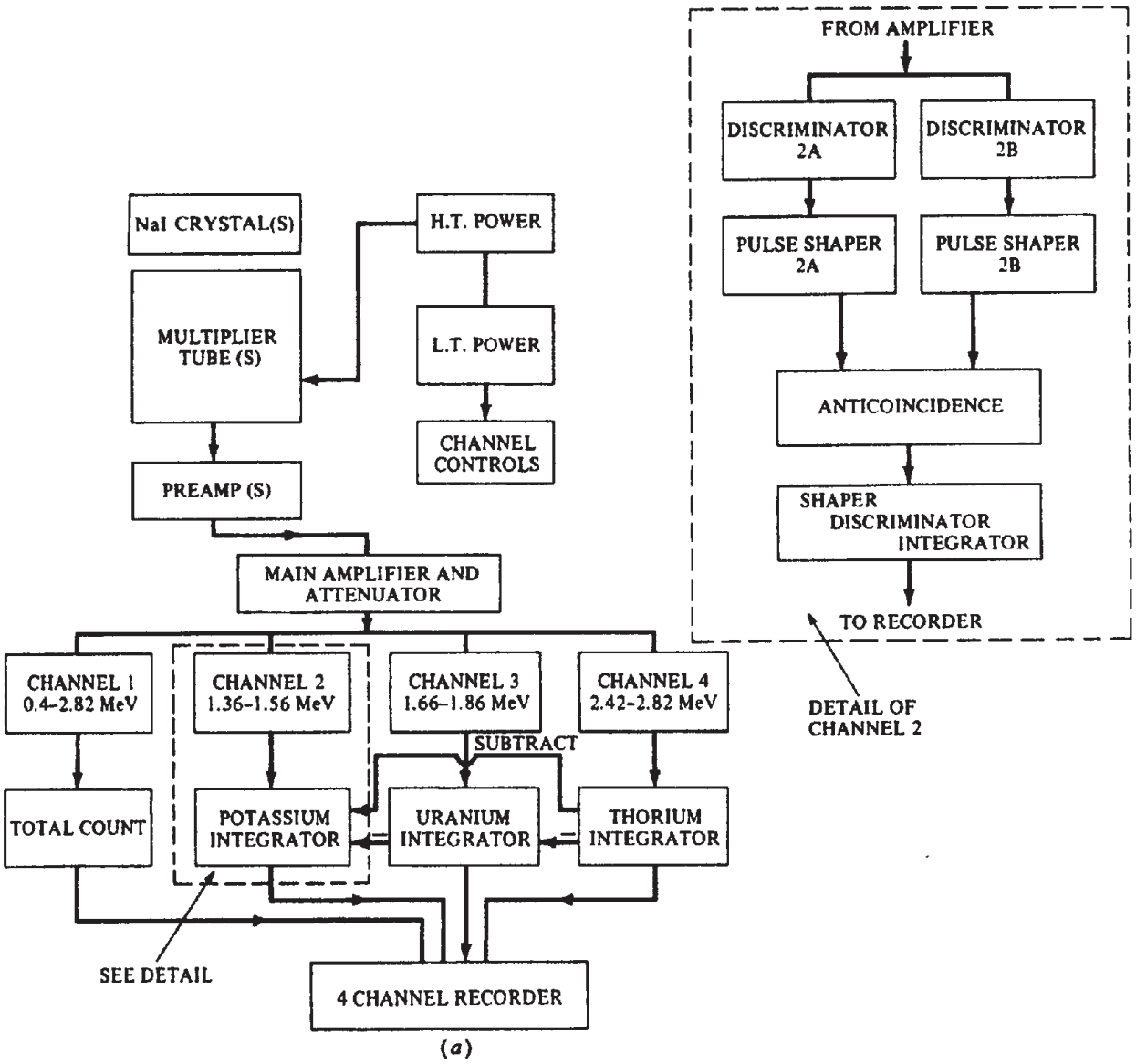

Figure 10.8. Four-channel γ-ray spectrometer. (a) Block diagram.

often contain both U and Th and even K as well, and because the count level may be considerably higher for one channel than the others (as in Fig. 10.7, where the count rate of the Th sample at 1.46 MeV, even in the absence of a peak, is more than 100 times larger than the potassium peak), some means of subtracting a predetermined fraction of the higher count rate, known as *spectral stripping*, is generally incorporated near the output end of the spectrometer, as shown by the subtract lines in Figure 10.8a. An early model of this type of instrument designed for airborne work is illustrated in Figure 10.8b. It employed twelve 9 × 4 in. (23 × 10 cm) crystals; the correct position of the channels was monitored with a Cs standard γ source (661 keV). Note that this instrument has four channels (Fig. 10.8a), channel 1 being for total count over the whole energy band from 0.4 to 2.8 MeV.

The block diagram in Figure 10.9 shows a more recent computer-controlled airborne system. Spectrometers with 256 and 512 channels have also been used in airborne surveys.

An inherent problem with the pulse-height analyzer is the effect of pulse shape, voltage drift, temperature changes, and so forth, on the instrument sensitivity and accuracy. Further improvements in instrumentation have resulted from using analog-to-digital (A/D) conversion and by incorporating a minicomputer to provide on-line data correction and ultimately interpretation during the survey. [For these and other developments in instrumentation, see Bristow (1979).] A glance at Figures 10.8 and 10.9,

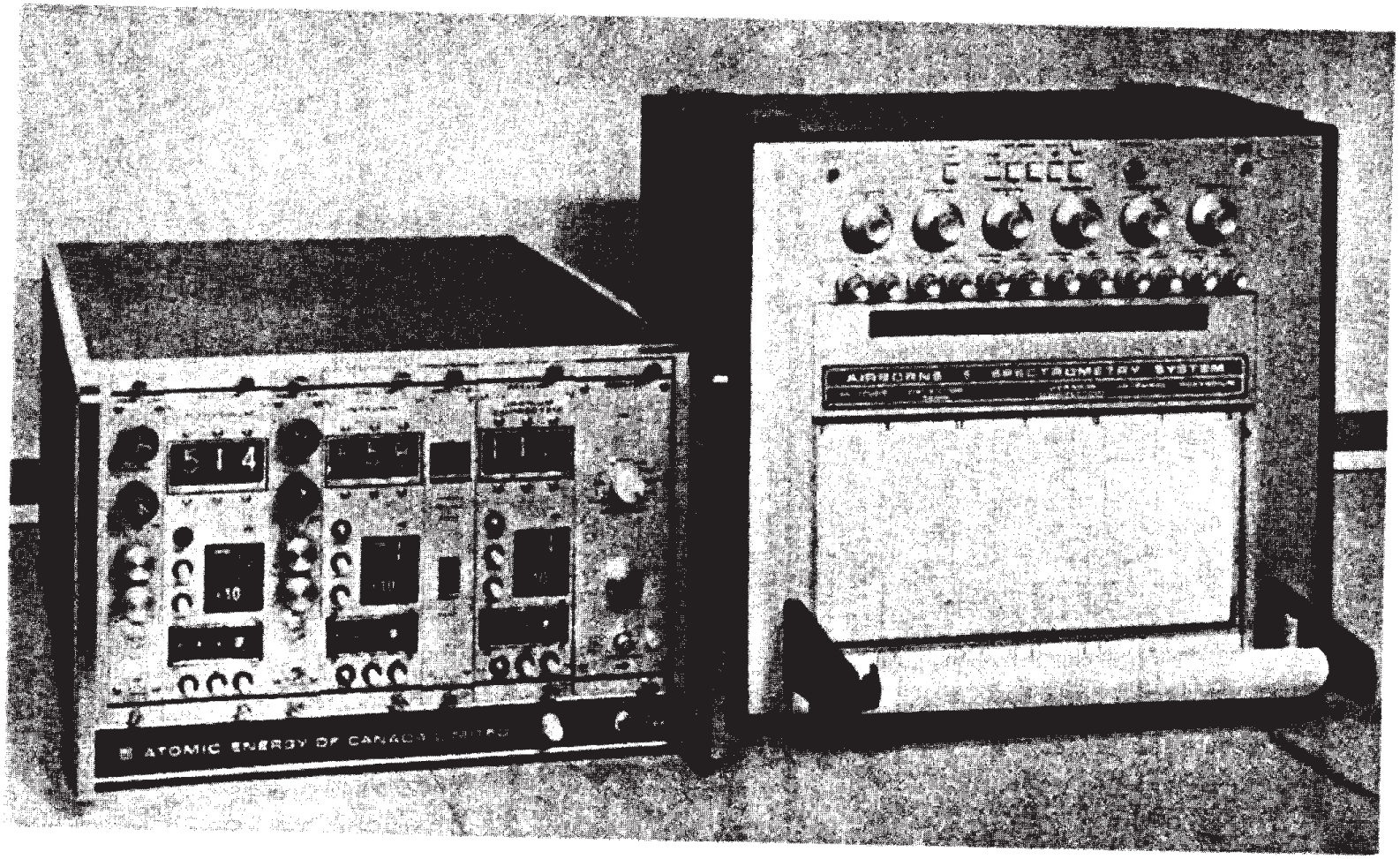

(*b*)

Figure 10.8. (Continued) (b) Photo.

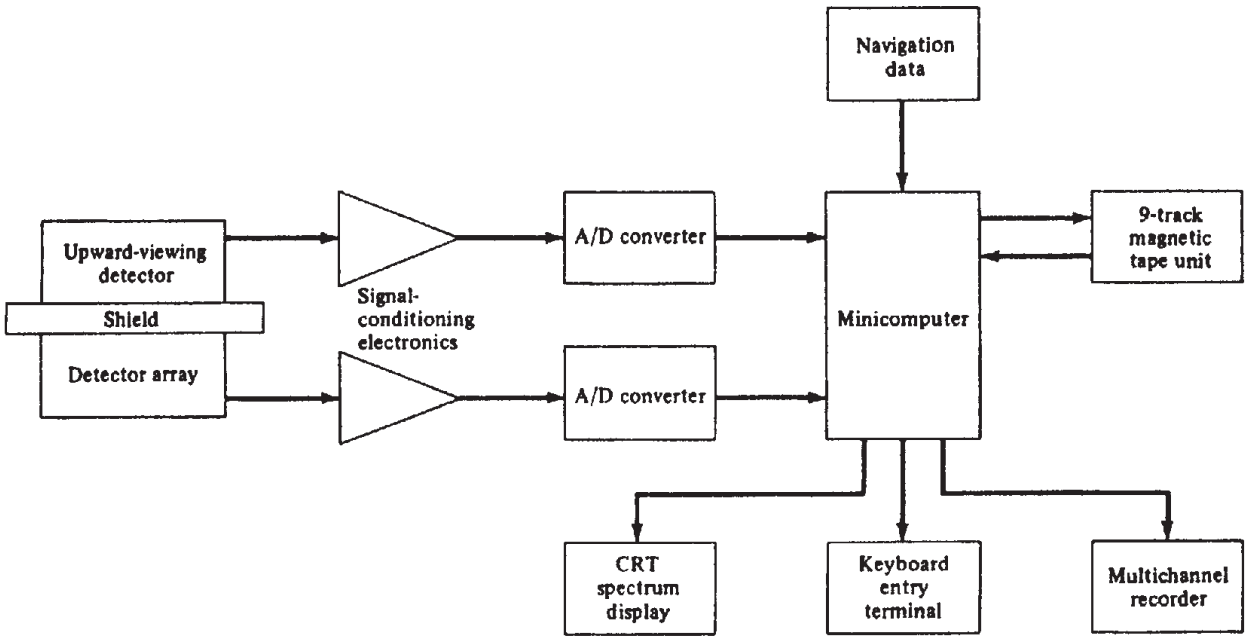

Figure 10.9. Modern γ-ray spectrometer. (After Bristow, 1979.)

the second displaying a block diagram of an up-to-date airborne installation, shows clearly that the present-day model is considerably more complex and sophisticated than the earlier one, employing as it does analog-to-digital conversion, a minicomputer, and consequent additional electronics, as well as an *upward-view detector*, shielded from ground radiation, to monitor atmospheric radiation. The computer is particularly attractive for storing useful control data to correct for background effect of atmospheric radon, which is erratic and often large.

10.3.5. Miscellaneous Instruments

Some portable scintillation meters have simple circuit modifications that permit rough discrimination between K, U, and Th, as well as measurement of total γ-ray count. A switch provides two bias levels on the pulse amplifier, equivalent to about 2.5 and 1.6 MeV, so that one can, in effect, introduce wide windows, one at a time, for Th and U + Th. Calibration of this type of equipment is discussed in Section 10.3.6.

An instrument known as the *emanometer*, or *radon sniffer*, has been used to measure the radon content of waters, oils, and soils. Because radon is a noble gas, it does not form chemical compounds. It moves freely through pore spaces, joints, and faults for distances up to several hundred meters. It will also dissolve in ground water and so move about in the subsurface.

Air samples are obtained from the soil by drilling a shallow hole (0.5 to 1 m) and pumping air from the hole through filters and a dryer into an ionization chamber or thin ZnS scintillator. Water samples are degassed and the gas–air mixture goes to the detecting chamber. In one model the 4.8 MeV α particles of ^{222}Rn are counted, rather than the 0.51 MeV γ ray.

If the radon is in equilibrium with the other decay products in the vicinity, the amount of parent product may be determined from Equation (10.5),

$$N_u = N_{rn}\lambda_{rn}/\lambda_u \approx 2 \times 10^{-6} N_{rn}/5 \times 10^{-18}$$
$$\approx 4 \times 10^{11} N_{rn}$$

assuming the radon originated from ^{238}U. The numerical factor would be about 4×10^{15} for radon gas from ^{235}U or ^{232}Th. These have very short half-lives, however; hence it is much more likely that ^{222}Rn is the isotope detected. If the series is not in equilibrium, for example, some member or members are reduced or missing because of weathering, and so forth, the count would be reduced and the preceding relation would not hold.

Two other integrating-type radon detectors, which collect and measure α radiation over much longer periods than the sniffer, have been in limited use since about 1978. The first, known as the *Track Etch*, consists of a cellulose nitrate film (sensitive to α particles) taped on the inside bottom of a plastic cup. The inverted cup is placed in a soil hole for about three weeks, accumulating α radiation inside from soil gas (the cup wall is thick enough to exclude penetration from outside). The film is retrieved, chemically etched to expose the α tracks, and the

amount of radiation is found from the track density viewed under a microscope.

The *Alpha Cup*, similar to the Track Etch in principle, uses a silicon semiconductor in place of the film. This detector is connected to an electronic unit outside the cup and the whole is buried for three days. After digging up the device, the α counts stored in the electronic memory are transferred to a reader. A later modification called *Alpha Card* appears to have better counting geometry, which reduces the burial period to 12 hr. This reduction in integrating times compared to Track Etch is said to be possible because of higher collection efficiency. The alpha devices also have an advantage, because there is no need to flush out the collector (required for cleaning out the sniffer) or change the detector after each station.

Because the radon diffusion process is complex and sensitive to several external factors, such as temperature, pressure, and climate, generally, one might expect that the long integration time would produce more reliable results. However, there is little available evidence to establish a definite superiority of one instrument over the others (Warren, 1977; Wollenburg, 1977; Telford, 1983).

A variety of other instruments has been developed for radioactivity measurements in geophysics. Several are adaptations of nuclear physics laboratory equipment for assaying. Others, such as the *beryllium detector*, used for ground prospecting, and the *density logger*, contain their own radioactive sources to initiate artificial radioactive processes in nearby rock. Some of these are discussed in Sections 11.8.3 and 11.8.4.

10.3.6. Calibration of Instruments

The calibration of instruments for reasonably quantitative measurements in radioactivity is a straightforward procedure in laboratory work, more complicated for field operations. For example, the scintillation meter described in Section 10.3.3c, may be adjusted to determine the relative amounts of uranium and thorium by means of a standard Th source and successive adjustments of the bias potentiometer control. When an instrument like the four-channel spectrometer is used in the field, however, a small standard source is quite unsuitable for overall calibration. Some of the difficulties encountered in stabilizing and calibrating multichannel spectrometers, particularly for airborne work, were mentioned briefly in Sections 10.3.3c and 10.3.4. Measures designed to resolve these difficulties included the stripping process and an upward view detector to correct for atmospheric radon background (see Fig. 10.9). An additional effect from cosmic-ray variations caused by terrain relief may be reduced by providing an extra energy window (3 to 6 MeV).

Clearly these background sources are larger and have higher intensity than laboratory standards, even though the count rate in the uranium window is the main concern for good calibration of the instrument. Two empirical techniques have been used to measure uranium background. The simplest is to fly over a lake, where the measured activity will be the total from K, U, and Th, but several orders lower than from the ground surface. An alternative is air sampling with filters, using an upward-view detector as in Figure 10.9; although not as reliable, this may be a necessity where reasonably sized bodies of water are not available.

For a satisfactory and complete spectrometer calibration, however, it is necessary to employ concrete structures of appropriate size as secondary standards for static calibration of ground, airborne, and borehole instruments, plus larger ground strips for test flights of airborne systems. The Geological Survey of Canada has five concrete slabs ($\sim 7.5 \times 7.5$ m, 0.5 m thick) at Uplands Airport near Ottawa. These contain varying fractions of radioactive material (for example 2.2% K, 3 ppm eU, 26 ppm eTh; see §10.5 for definition of eU and eTh) and are suitable for calibration of ground and airborne equipment. At the same location nine concrete test columns with standard size boreholes are available for calibrating logging instruments. Ground strips for flight tests are also installed near Ottawa. Similar installations exist in the United States and several other countries.

10.4. FIELD OPERATIONS

Ground prospecting is readily carried out with any of the instruments described in Sections 10.3.2 to 10.3.5. The Geiger counter is used only for foot traverses; the scintillometer and γ ray spectrometer, especially the former, may also be used in vehicles. Radiometric surveys are comparatively cheap, whether airborne or on the ground (see §10.1); in surface work this is partly because the line cutting is often unnecessary and measurements are simple and rapid. No particular expertise is required for this work. It is sufficient to note the count rate (counts/s, mr/hr) of the instrument and compare it with a background reading. Ratios $> 3:1$ over background would generally be of interest.

The background itself may vary considerably from place to place, depending on depth of soil cover and potassium content of the local rocks. Some notice must be taken of the geometry of outcropping formations in this regard, because the instrument response is influenced by source–detector separation

and the source dimensions. This is particularly true of the Geiger counter. Obviously the source–detector geometry will have a significant effect on the readings; compared to the usual position of the instrument over a flat surface (2π geometry), a wide ledge backed by a vertical wall (3π) or a steep road cut ($\sim 4\pi$) will increase response by 50 to 100%.

Background variation in different rocks has already been referred to in Table 10.5. In the early days of radioactive prospecting, erratic increases in background occurred occasionally as a result of atomic tests; this is no problem nowadays.

Two good reports on γ-ray spectrometric methods for uranium – airborne, ground, and well-logging – may be found in Grasty (1979) and Killeen (1979). Airborne radiometric reconnaissance has frequently been accompanied by aeromagnetics and occasionally EM. This stage is generally followed by detailed ground radiometric coverage of favorable areas, possibly with geochemical sampling, auxilary geophysical methods, and finally trenching and drilling plus γ-ray logging. When the survey area is small or difficult for ground access, a detailed airborne helicopter survey may be warranted to reduce the ground followup.

Airborne radioactivity surveys have been carried out for minerals other than uranium and thorium, such as titanium and zirconium-bearing heavy minerals, including tantalum, niobium, and the rare earths. In this connection carbonatites (such as at Oka and other locations in the province of Quebec) are an intriguing target for γ-ray spectrometer exploration because they have a very low ratio of uranium to thorium. This distinctive signature applies to kimberlites as well; hence the method is useful in prospecting for diamonds.

Limited attempts have been made to use the radioactivity method in oil exploration. Surveys in known oil fields sometimes indicated a radioactive low directly over the oil-bearing structure with a halo slightly above the background surrounding it. Actually this pattern was reported about 1928 from crude ground surveys in Texas fields. The source of radioactivity appears to be radon gas, which moves upward through fractures in the perimeter rock to escape at surface; the suggestion has been made that the tight cap rock over the oil pool is relatively impervious to this migration.

Other indirect applications that may be worthwhile are in relation to phosphorites, whose host rocks often are anomalous in uranium content, and even for sulfides. Also, radiometrics occasionally have been used as an aid to geological mapping; a case history using airborne data is illustrated in Section 10.6, example 1. These indirect applications of radioactivity will be discussed further in Section 10.5.

10.5. INTERPRETATION

In spite of great improvements in instrumentation, the interpretation of radiometric survey data is still mainly qualitative. This is partly due to the extremely small depth of penetration possible with the method. It is also the result of the inherently complex nature of the γ-ray spectra.

Spectrometer profiles taken in a helicopter are illustrated in Figure 10.10a. Altitude in both cases was 150 m. The low air speed possible with the helicopter (40 km/hr) is a decided advantage both for amplitude of response and discrimination of anomalies. This was an early test of the four-channel spectrometer. Its superiority over instruments providing only total-count data is clearly demonstrated in Figure 10.10b where the strong U anomaly marked by the arrows is lost in the total-count (integral) profile because K and Th responses are low over the same 5 km stretch of the profile.

Both airborne and ground spectrometer data may be plotted as profiles or contoured as shown in various diagrams of Sections 10.6 and 10.7, in terms of U, Th, K, and total counts per second, ratios of U : Th, U : K, or in relation to some arbitrary background.

Uranium and thorium amplitudes may also be given as eU and eTh; that is, *equivalent uranium* and *thorium*. These designations arose because in γ-ray spectrometry the elements actually measured in the 1.76 and 2.62 MeV channels are ^{214}Bi and ^{208}Tl, respectively, rather than their U and Th parents. The distinction obviously is unnecessary for K because it is measured directly in the 1.46 MeV channel.

Some attempts have been made to obtain quantitative results in airborne work. By correlation of detailed ground data with airborne surveys over the same area, it is possible to get an approximate fit between the airborne profiles and upward continuation of the ground data, using an empirical expression for the γ-ray attenuation in air (Soonawala, 1968). This correlation is reasonably valid because of the high attenuation in solid material; that is, the source must outcrop to be detected in either survey. Characteristic curves for elementary shapes are then drawn up for the airborne interpretation in other areas. Three elementary geometries are considered:

1. A finite or elementary circular source.
2. An infinite plane source (outcrop) of great lateral extent.
3. The line source, having infinite exposed length along one axis, considered to be the strike direction.

Clearly the finite source is the most usual geometry encountered in the field, because either of the

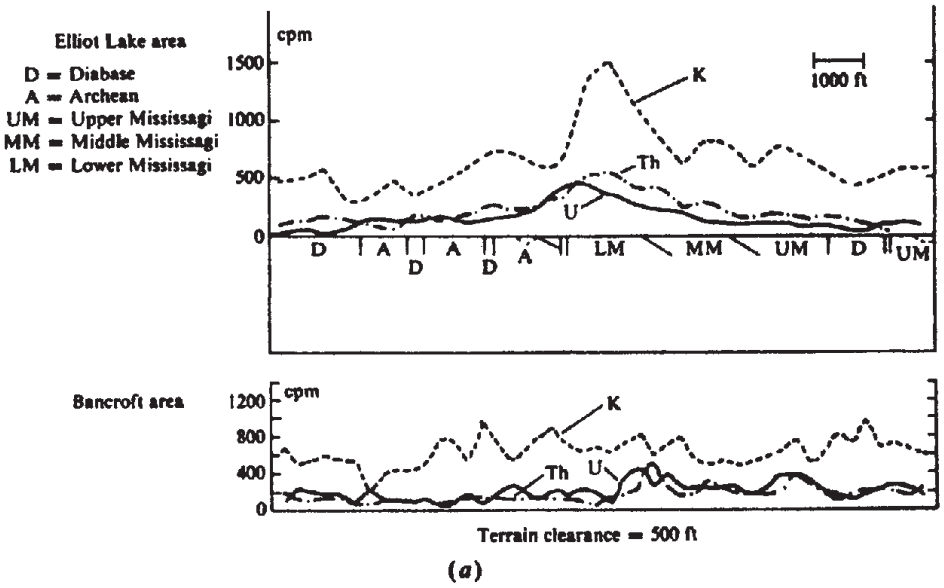

(*a*)

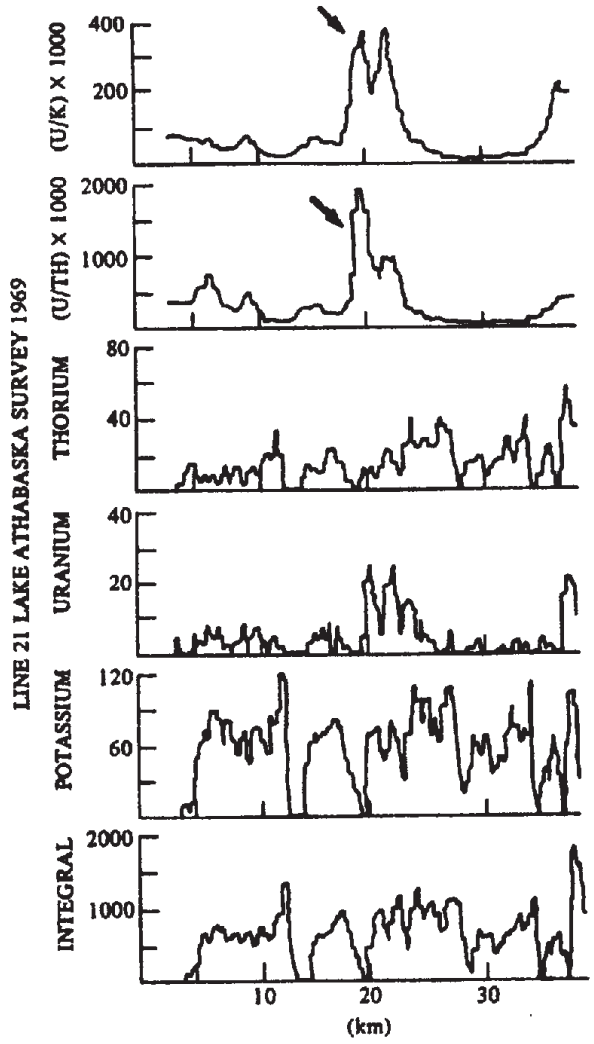

(*b*)

Figure 10.10. Airborne γ-ray spectrometer profiles. (a) Total-count profiles in the Elliot Lake and Bancroft areas, Ontario. (b) Four-channel results, Uranium City area, Saskatchewan. (After Darnley, 1970.)

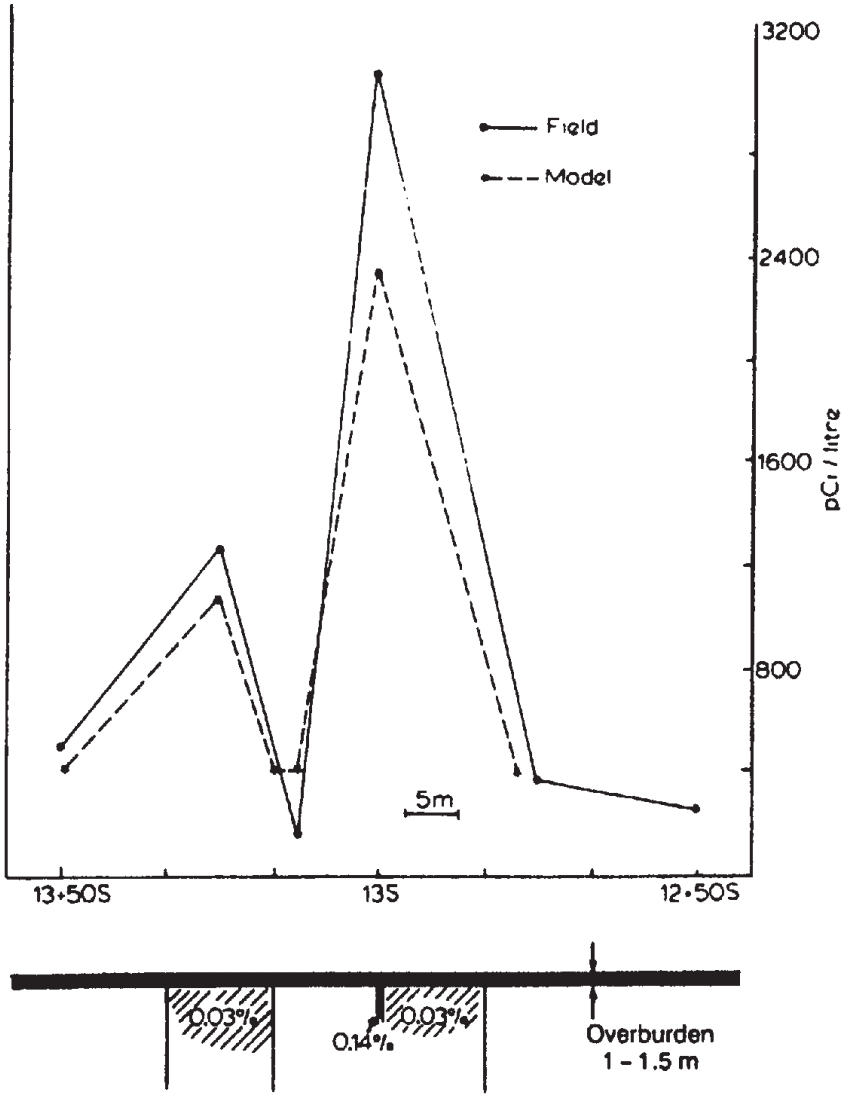

Figure 10.11. Radon profile and model results, Northern Saskatchewan. (From Soonawala, 1976.)

others will generally be covered with overburden at various places. Practically, the elementary source need not be circular, but its largest dimension should not greatly exceed the altitude of the aircraft.

The characteristic curves enable us to determine a parameter involving the product of surface area and source intensity; these quantities (as in gravity, EM, and other situations) cannot be resolved individually.

Measurement of the K, U, and Th γ-ray peaks in the 1.46, 1.76, and 2.62 MeV energy windows, together with U : K and U : Th ratios plus total count (using a four-channel spectrometer) is only a first approximation to a quantitative determination of relative ground abundance of the three elements. The numerous background variables, some of which have been mentioned already, include source–detector geometry, sampling rates, aircraft altitude, radioactive equilibrium, Compton scattering, and cosmic and atmospheric radon background.

Crossley and Reid (1982) used a matrix equation (see §A.2) to solve for the abundances

$$\mathscr{A}\mathscr{X} = \mathscr{C}$$

where $\mathscr{X}$ is an $(m \times 1)$ matrix of the abundances, the $(n \times 1)$ matrix $\mathscr{C}$ gives the counts in the n channels, and $\mathscr{A}$ is an $(n \times m)$ matrix of the calibration constants. For three-channel equipment the elements a_{ij} are stripping constants (see §10.3.4 and problem 4) for K, U, and Th.

To improve the accuracy, we must use more than three channels. Crossley and Reid (1982) used data from 63 channels in the range 0.78–2.98 MeV (n = 63) to solve for K, U, Th, and cosmic background

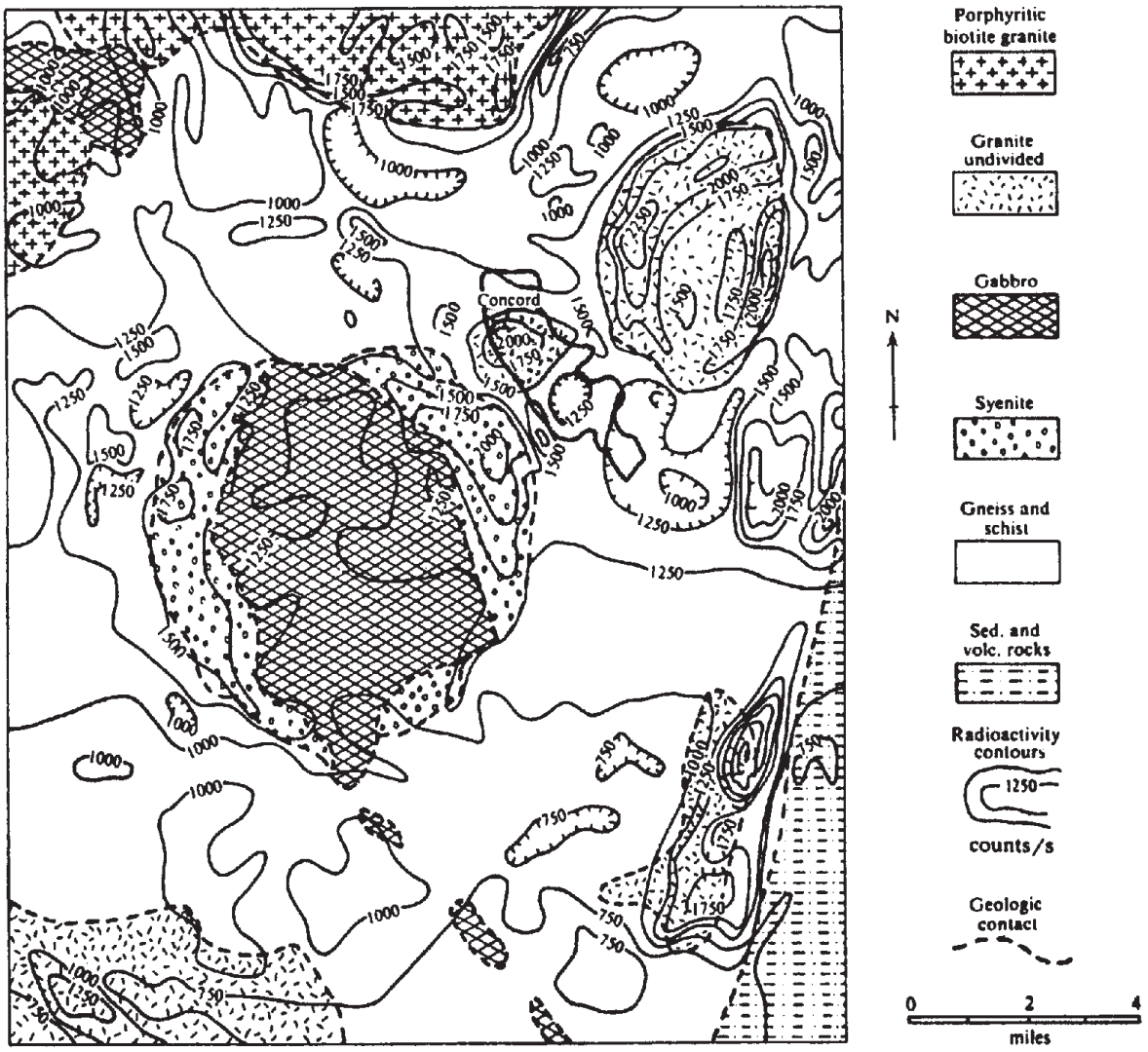

Figure 10.12. Airborne radiometrics as an aid to geological mapping, Concord Quadrangle, North Carolina. (After Bates, 1966.)

abundances ($m = 4$); because $n > m$, they used a least-squares solution (§A.8). The results indicated that a full-spectrum multichannel matrix solution was desirable, particularly additional U and Th windows at 1.12 and 0.94 MeV, respectively, well below the usual 1.76 and 2.62 MeV windows. They also found that the cosmic background varied appreciably over periods of a few seconds; this might be significant in calibrating equipment by flying over lakes (although their assumed cosmic data might include other background effects not taken into account, that is, $m > 4$).

Analytic work involving diffusion and convection of radon through overburden has led to numerical methods for modeling various geometries such as 2-D and 3-D blocks under overburden (Soonawala, 1976; Soonawala and Telford, 1980). The treatment is similar to that used in EM and MT analysis. Figure 10.11 shows an example in which a thin zone of 0.14% U, 0.5 m wide, surrounded by a 0.03% halo, all under 1 m overburden, was used to match a field profile; the anomaly had been partly confirmed by previous drilling.

Use of the radioactivity method in exploration for petroleum and natural gas was mentioned briefly in Section 10.4, where the anomaly and its possible mechanism were described. An early reference to this technique is given by Sikka (1959), who analyzed radiometric contours from an airborne test survey over the Redwater oil field near Edmonton, Alberta. The area was flown twice, first in 1951 with a scintillometer measuring total count, and again in 1957 using a total-count γ-ray instrument that also recorded energies above 1.5 MeV, thus eliminating the effect of ^{40}K (see problem 5).

Recent applications of this method are reported in Weart and Heimberg (1981). They measured total γ-ray count in a large ionization chamber from a

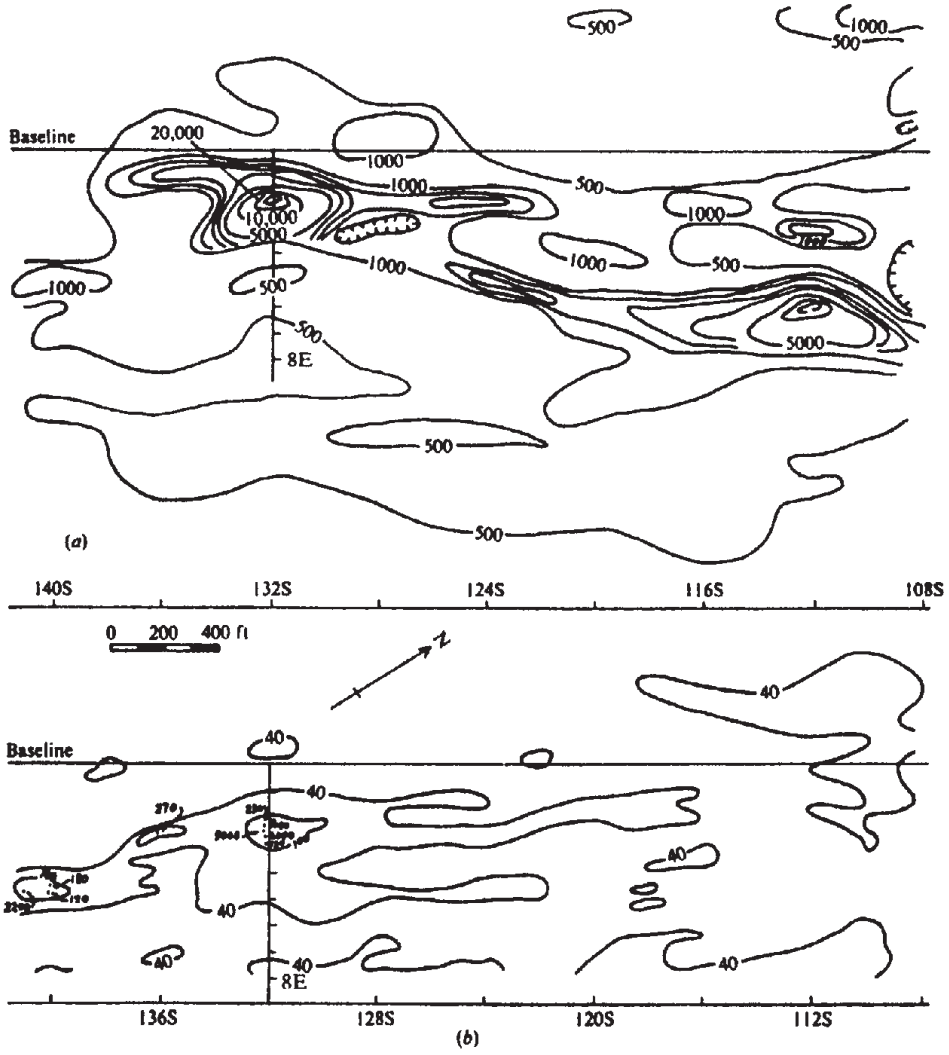

Figure 10.13. Uranium exploration using ground magnetics and radiometrics. (a) Magnetic contours (nT). (b) Radioactivity contours (total γ-ray flux in counts/s).

vehicle or on foot where access was difficult. Surveys were carried out in six states (United States) generally before, in some cases after, drilling. Of some 1,000 wells drilled, about 750 are reported to have been correctly predicted, either as producers or dry, by their location with respect to the radiometric survey data; this compares favorably with domestic drilling statistics for oil and gas. Curry (1984) gives somewhat similar results for about 500 wells in the Powder River Basin area of Wyoming.

Limited tests with ground radon detectors for shallow structural mapping have been reported. King (1978) measured ^{222}Rn on the San Andreas fault in California. Soonawala (1976) obtained feeble radon anomalies across fault planes in the Eldorado area, northwestern Canada, about the magnitude expected from diffusion theory; the fault response, however, was contaminated by mining activity, because there are several major orebodies nearby. Abdoh-Reza (1984) measured distinctive anomalies over faults in the vicinity of Ile Bizard, west of Montreal. The clarity of response here, compared to that obtained by Soonawala, is probably the result of much lower background radiation in this area.

Airborne radiometrics have occasionally been used as an aid in geological mapping; a case history is discussed in the next section. An attractive color map for this purpose was recently reported by the U.S. Geological Survey (Duval, 1983). A composite color image contour map is produced by combining any three K, U, Th parameters, or their ratios. Anomalous areas may be shown either as dark zones, known as *direct image displays*, or bright sections, called *inverse images*. This type of reproduction at both ends of the visible spectrum is said to offer more complete sensitivity to the eye for interpretation. Judging by an example of the color maps from an area in southeast Texas, the technique might have

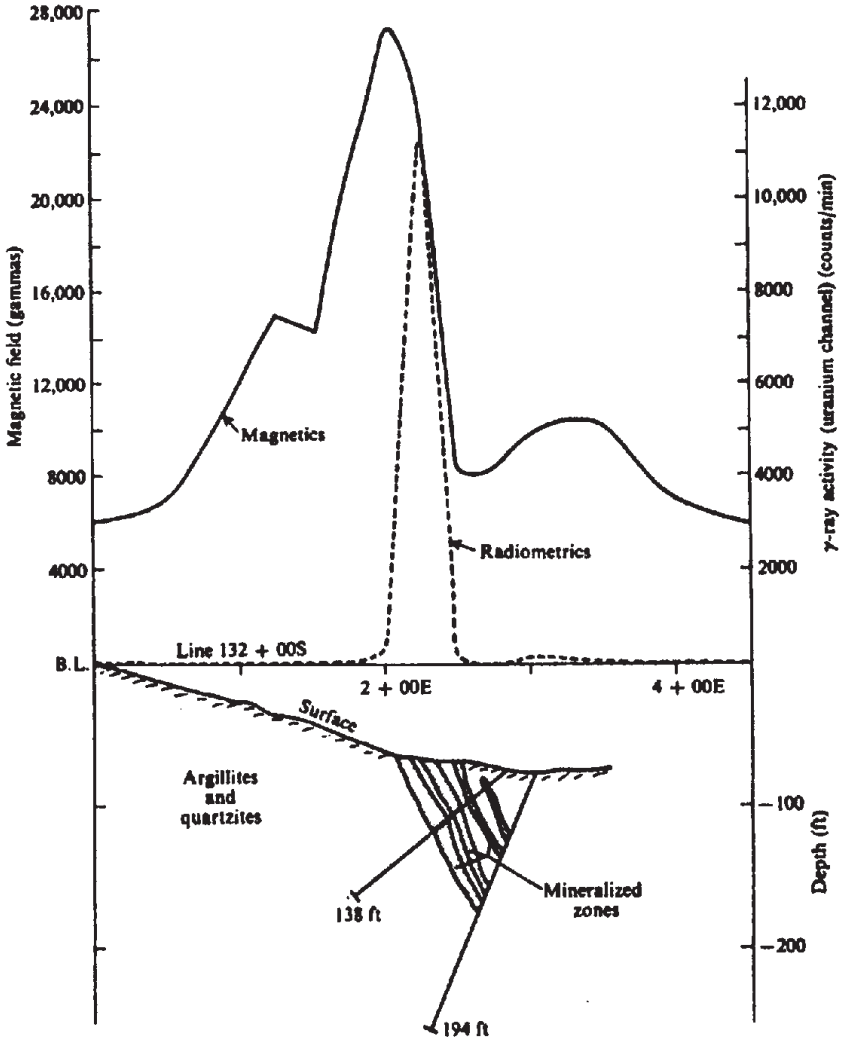

Figure 10.14. Radioactivity and magnetic profiles plus geologic section, line 132 + 00S, uranium survey.

limited application in mapping and qualitative interpretation of surface geology.

10.6. FIELD EXAMPLES

1. Figure 10.12 illustrates the application of airborne radioactivity to geologic mapping. The area shown is the Concord quadrangle of North Carolina, where the U.S. Geological Survey carried out an airborne radiometric survey as an aid to detailed mapping of complex geology. Six NaI crystals, 10 cm diameter, 5 cm thick, and six photomultiplier tubes connected in parallel were used for the detector. Particular care was taken to correct the data for variations in aircraft altitude.

The compilation of geologic and radioactivity information in Figure 10.12 represents a progressive refinement of data; that is, the original geologic information was changed as a result of additional geologic mapping, which was to a considerable extent guided by the radioactivity results. For example, the radiometric survey outlined a granite stock, northeast of the town of Concord, whose borders could not be well defined by field geology; it also located the smaller granite body in the northwest part of the town.

The granitic zone in the southeast corner of the figure is marked by high radioactivity, whereas that on the southwest is not. A porphyritic biotite granite in the northern part of the quadrangle shows medium to high radioactivity, but in the vicinity of the gabbro mass in the northwest corner the response is lower. The anomalous high along the east border coincides with a considerable injection of granite into the surrounding gneiss and schist. Finally, the large gabbro-syenite mass in the center of the quadrangle is fairly well outlined by the radioactivity contours, because the syenite zones on the east and west flanks show higher response than either the gneiss-schist surroundings or the enclosed gabbro.

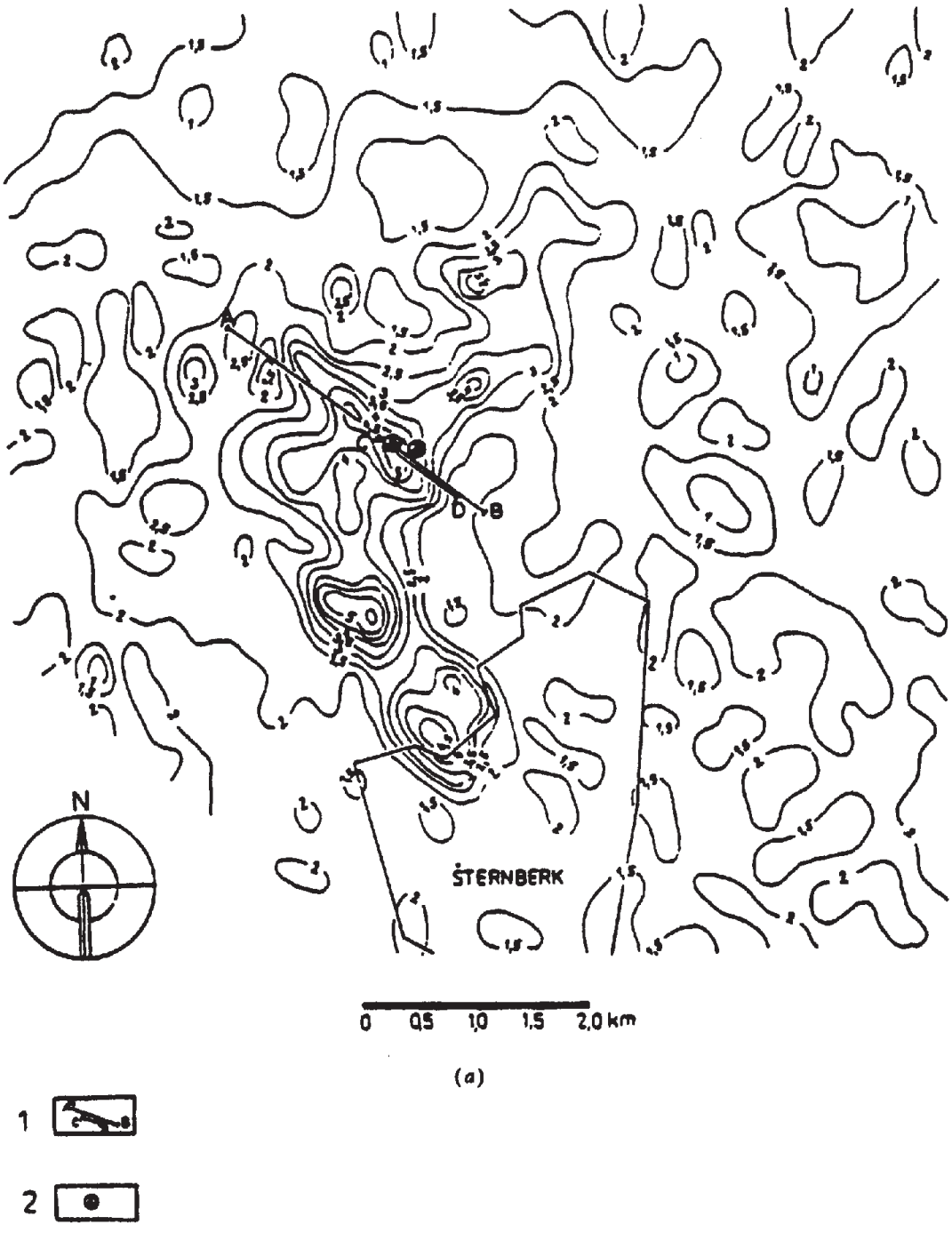

Figure 10.15. Airborne survey for potassium used to locate associated Zn mineralization. (After Gnojek and Prichystal, 1985.) (a) ^{40}K contours, contour interval 0.5%; • mark two drillholes.

The variation in radioactivity response over different granitic zones is not definitely explained, although it is suggested that there may be different types of granite within the quadrangle. No mention is made of the depth of overburden; slight variations in the thickness or type of cover could account for the lows in the northwest and southwest corners.

Neither the airborne radiometrics nor the geologic mapping could have produced this interpretation independently. It is the product of a combination of the two, plus some aeromagnetic data. Furthermore, the airborne survey, as mentioned previously, was useful in selecting areas for further detailed mapping, thus saving time and money.

2. An example of the direct method of radioactivity prospecting is shown in Figure 10.13 and 10.14 taken from an extensive survey for uranium in

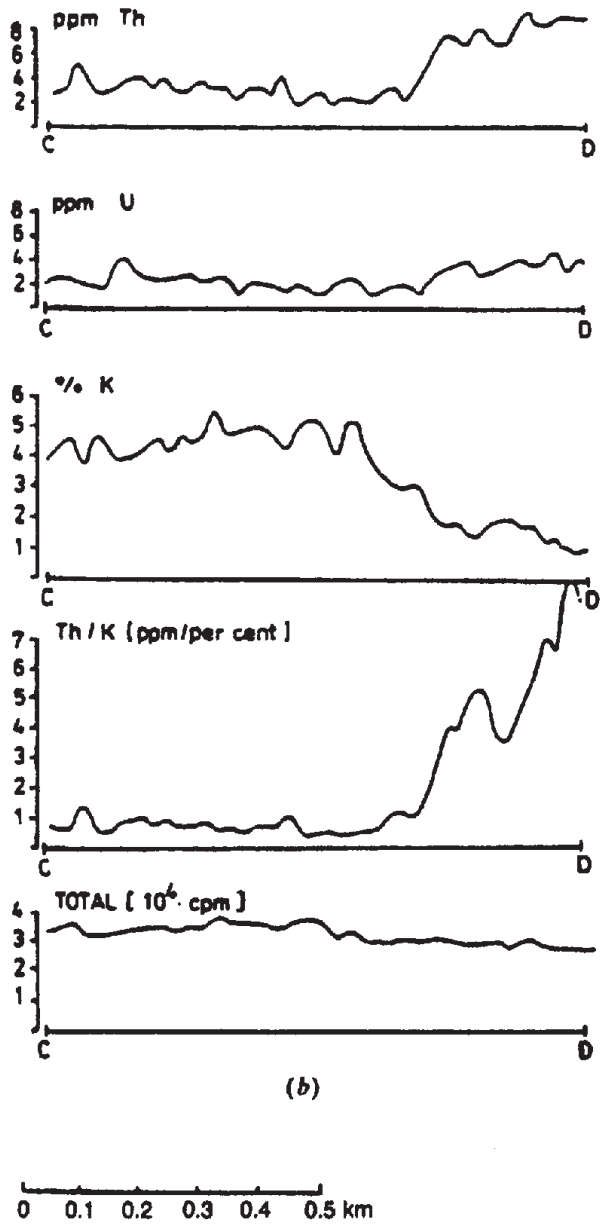

Figure 10.15. (Continued) (b) Th, U, K, Th/K, and total-count profiles on line CD [see part (a) for location].

Labrador. Following large-scale reconnaissance with airborne radiometrics and magnetics, a set of targets was selected for detailed ground followup. The latter operation proceeded in two steps. First, the airborne radioactivity anomalies were located and assessed roughly; then the more promising of these were examined in detail by scintillometer and magnetometer (in some cases ground EM was also employed, because there were sulfides associated with the radioactive minerals). Stations were 10 to 25 ft apart along cut lines spaced 100 ft apart.

Figure 10.13 shows the radioactivity and magnetic contours for a small area of the ground survey. Strong anomalies of both types are coincident on L132S at 2E. These were indicated by the airborne survey, the location being almost exactly the same as the ground anomaly. At L112S, 6E, however, there is no abnormal radioactivity associated with the high magnetics.

Magnetic and radiometric profiles on L132S (the latter being obtained by using the uranium channel on the scintillometer), together with a vertical geologic section obtained from drilling, are displayed in Figure 10.14. The host rocks are argillites, quartzites, and amphibolites. The mineralization, consisting of magnetite and pitchblende with some chalcopyrite, sphalerite, and pyrrhotite, occurs in bands of ferruginous quartzites which alternate with diorite dikes. The overburden at the collars of the two drill holes is about 2 m thick and the huge magnetic and γ-ray peaks occur directly over exposed mineralization.

Although the U_3O_8 mineralization is probably of economic grade, the volume is small. The maximum depth extent is 40 m, whereas additional drilling showed the zone width and strike length to be no greater than 3 m and 75 m, respectively. Although the contours of Figure 10.13a and b indicate the small lateral extent of the showing, this evidence is not conclusive in itself for two reasons: first, a meter of overburden would be sufficient to mask the presence of uranium; second, the association of Fe_3O_4 and U_3O_8 mineralization does not prevail throughout the area, as proved by drilling in the vicinity of the magnetic anomaly near 6E on L112S.

3. Gnojek and Prichystal (1985) report the detection of zinc mineralization in northern Moravia by potassium anomalies from airborne γ-ray spectroscopy. Hydrochemical and self-potential anomalies accompanied by tectonic considerations had shown that sulfides might be present in the area. The airborne survey was carried out with a four-channel spectrometer and a magnetometer in a helicopter at 80 m ground clearance with 250 m line spacing. Two distinct ^{40}K anomalies of $\geq 5\%$ were detected, accompanied by variable U and very low Th.

The anomalies were verified by ground followup using radiometrics, a variety of electrical methods, and geochemistry. Despite the presence of basic rocks, there were no magnetic anomalies. The ^{40}K data provided locations for drilling, which encountered ZnS at 150 and 75 m depths in two holes. Figure 10.15a displays contours of ^{40}K over the area and the borehole locations, and Figure 10.15b shows various concentrations from a profile along line *CD*. The latter again illustrates the superiority of separate K, U, and Th measurements over total count.

Unless this example is an isolated case, the use of radometric surveys for base-metal and other mineral targets may be useful, particularly in areas where

Table 10.6.

Station	Lines							
	1	2	3	4	5	6	7	8
1	11	11	11	12	11	12	14	15
2	12	12	11	12	12	15	15	17
3	14	14	12	14	14	17	17	17
4	17	15	15	15	15	24	17	17
5	19	18	18	18	17	34	22	16
$5\frac{1}{2}$	—	30	21	24	22	—	—	—
6	16	25	24	23	28	47	27	18
7	17	23	25	28	34	47	30	24
8	16	17	30	36	46	66	47	38
$8\frac{1}{2}$	—	—	—	70	200	—	66	60
9	15	22	36	1,200	200	310	260	40
10	14	18	22	50	35	35	46	25
11	13	15	18	22	26	26	33	17
12	12	12	15	18	17	17	14	13

normal techniques are ruled out by high electrical noise.

10.7. PROBLEMS

1. Scintillometer readings were taken at station intervals of 8 m on a set of parallel lines 8 m apart over an area in Saskatchewan during the course of a uranium exploration program. The readings, in counts per minute, are given in Table 10.6.

   Plot and contour these readings; estimate the strike and width of the anomalous zone. Are there indications of the depth of overburden and variations of the overburden thickness in these values?
2. A 2.5 kg rock sample was tested for radioactivity with a scintillometer, both being enclosed in a large shielded container. The average count rate was 540 cpm. The background count in the container was 35 cpm. Assuming the overall efficiency of the scintillometer to be 30%, and either that the radioactivity is approximately equally distributed between uranium, thorium, and potassium or that there is no potassium in the rock and the U : Th ratio (§10.5) is about 0.5, determine the content of each element in the sample for the two cases (see Table 10.2, §10.2.4).
3. Scintillometer and vertical-component magnetic contours, taken from a detailed ground survey for uranium in northern Canada are shown in Figure 10.16. An excerpt from the geological report on the region says: "Geologically these areas are quite featureless and consist of pink quartzites with dark bands of mafic minerals, the latter coinciding with the radioactivity and magnetic anomalies at a number of places."

   Make an interpretation of this small section using the limited data available and keeping in mind possible coincidences of magnetic and radiometric anomalies, variations in depth of overburden, presence of granitic rock (^{40}K radioactivity), and so forth. As an aid to interpretation, it is suggested that the two contoured maps be overlaid and also that a few profiles be taken off each map.
4. As mentioned in Section 10.3.4, the present type of γ-ray spectrometer has three channels at 1.46, 1.76, and 2.62 MeV to isolate K, U, and Th peaks, respectively. Consequently it is possible to determine the individual amounts of potassium, uranium, and thorium contained in a rock sample when the spectrometer has been calibrated by using standard samples of known composition. We obtain the relative content of the three elements in terms of the count rates of the instrument as outlined in the following text.

   None of the γ rays from uranium or potassium has sufficient energy to be recorded in the thorium (2.62 MeV) channel; hence

$$T = k_1 T_c$$

   where T is the thorium content in parts per million, T_c is the 2.62 MeV channel count rate less background, and k_1 is the constant for the thorium channel.

   The 1.76 MeV uranium channel records γ radiation for uranium and thorium but none from potassium. Hence we have

$$U = k_2(U_c - S_1 T_c)$$

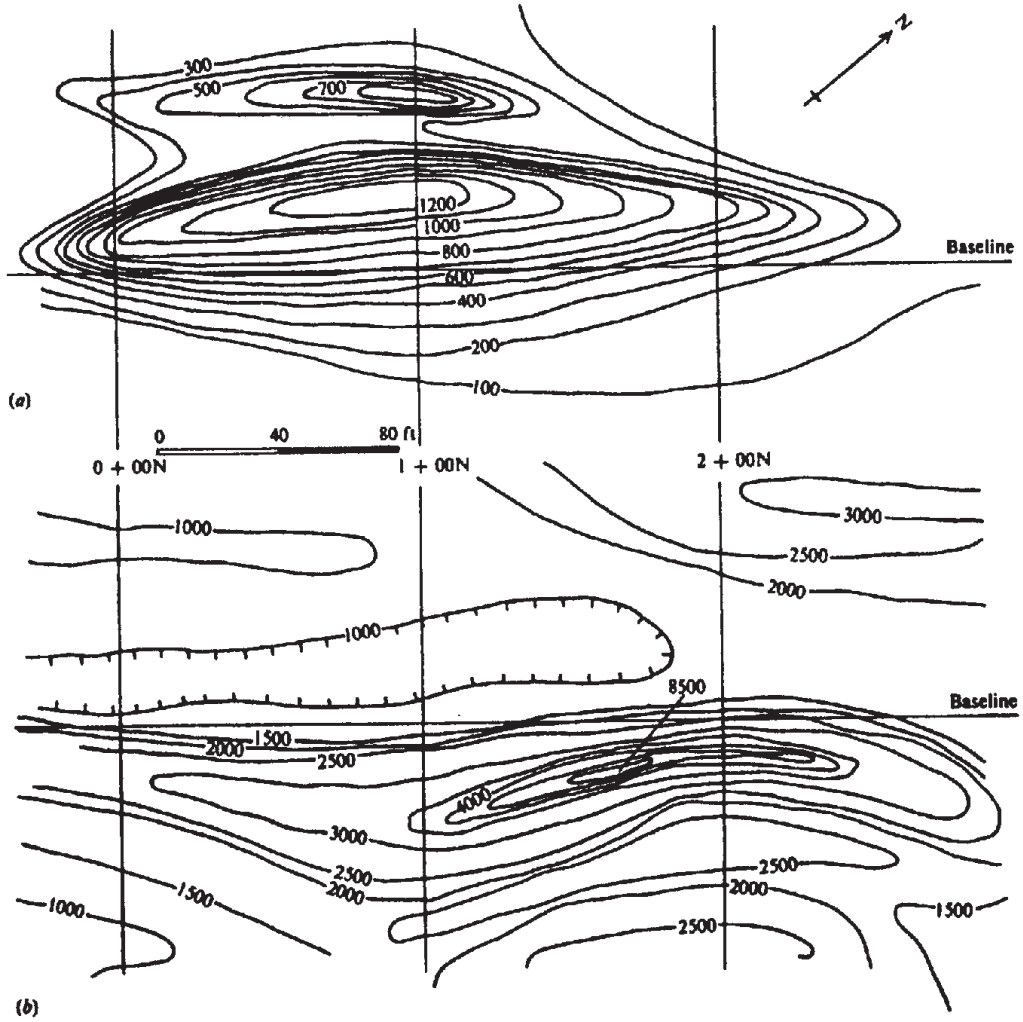

Figure 10.16. Radioactivity and magnetic contours, Northern Canada. (a) Wide-window γ-ray flux (counts/s), background 60 counts/s. (b) Vertical-component of the magnetic field (gammas).

where U is the uranium content in parts per million, k_2 is the constant for the uranium channel, U_c is the 1.76 MeV channel count rate less background, and S_1 is the stripping constant for thorium γ rays in the uranium channel (see next paragraph).

Finally, in the 1.46 MeV potassium channel we may have counts from uranium and thorium as well as potassium. The potassium content, $K_{\%}$ (expressed as a percentage because it is generally much larger than the amounts of U and Th), is given by

$$K_{\%} = k_3\{K_c - S_2(U_c - S_1T_c) - S_3T_c\}$$

where k_3 is the constant for the potassium channel, K_c is the 1.46 MeV channel count rate less background, and S_2, S_3 are the stripping constants for U and Th γ rays in the K channel. Because the γ-ray spectrum of an element is invariant, the stripping constant is merely the fixed ratio of the count rates for U or Th at the appropriate energy levels; thus, S_1 is the ratio of the count rates for Th in two channels centered at 1.76 and 2.62 MeV; hence multiplying the observed count rate for the 2.62 MeV channel by S_1

Table 10.7.

Station (ft)	Spectrometer readings (cpm)		
	T_c	U_c	K_c
0	13	28	195
100	8	27	243
170	22	34	265
200	25	36	218
210	18	30	135
230	10	24	223
300	15	27	193
400	15	30	197
425	12	20	242
500	8	21	233

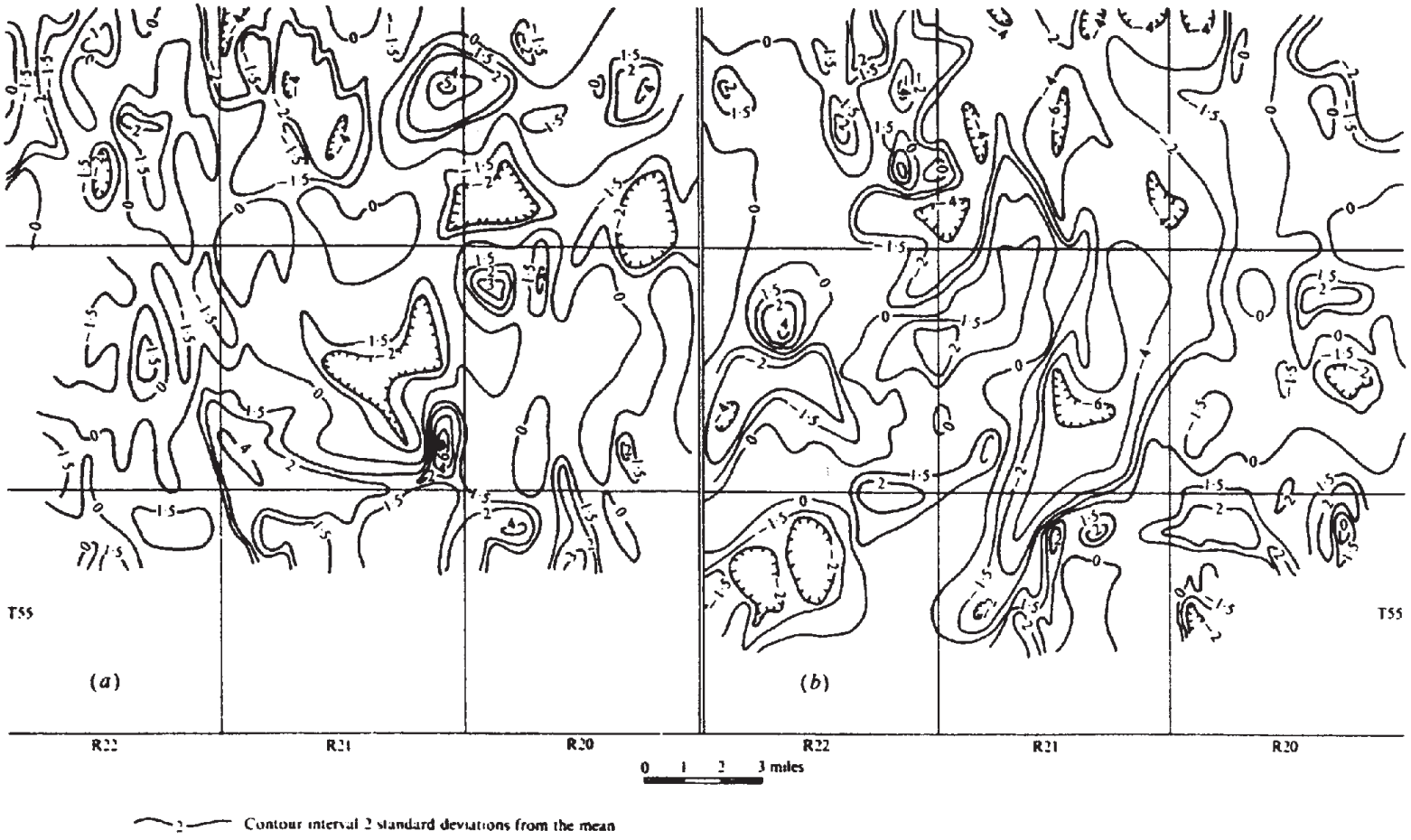

Figure 10.17. Aeroradiometric survey, Redwater Oilfield, Alberta. (a) Area flown east – west, winter of 1957; contours are total-count for energies above 1.5 MeV. (b) Area flown east – west, autumn of 1951; contours are for total count only.

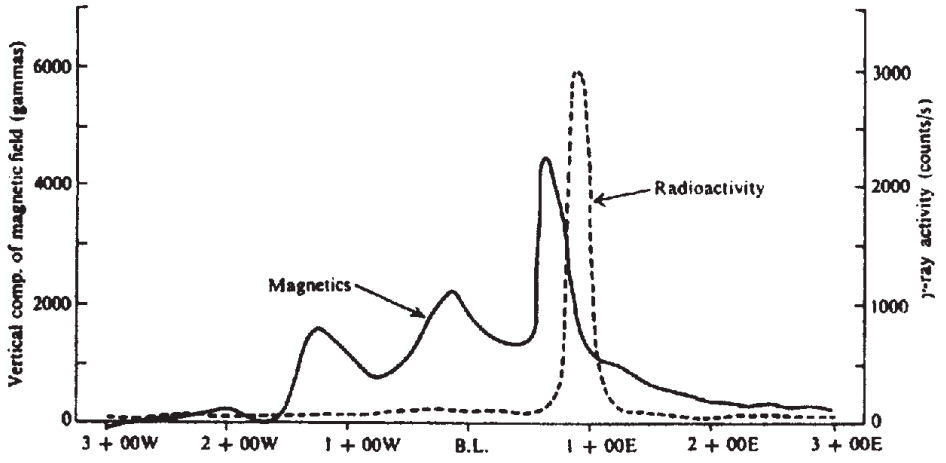

Figure 10.18. Radiometric and magnetic profiles from a survey for base-metals plus uranium.

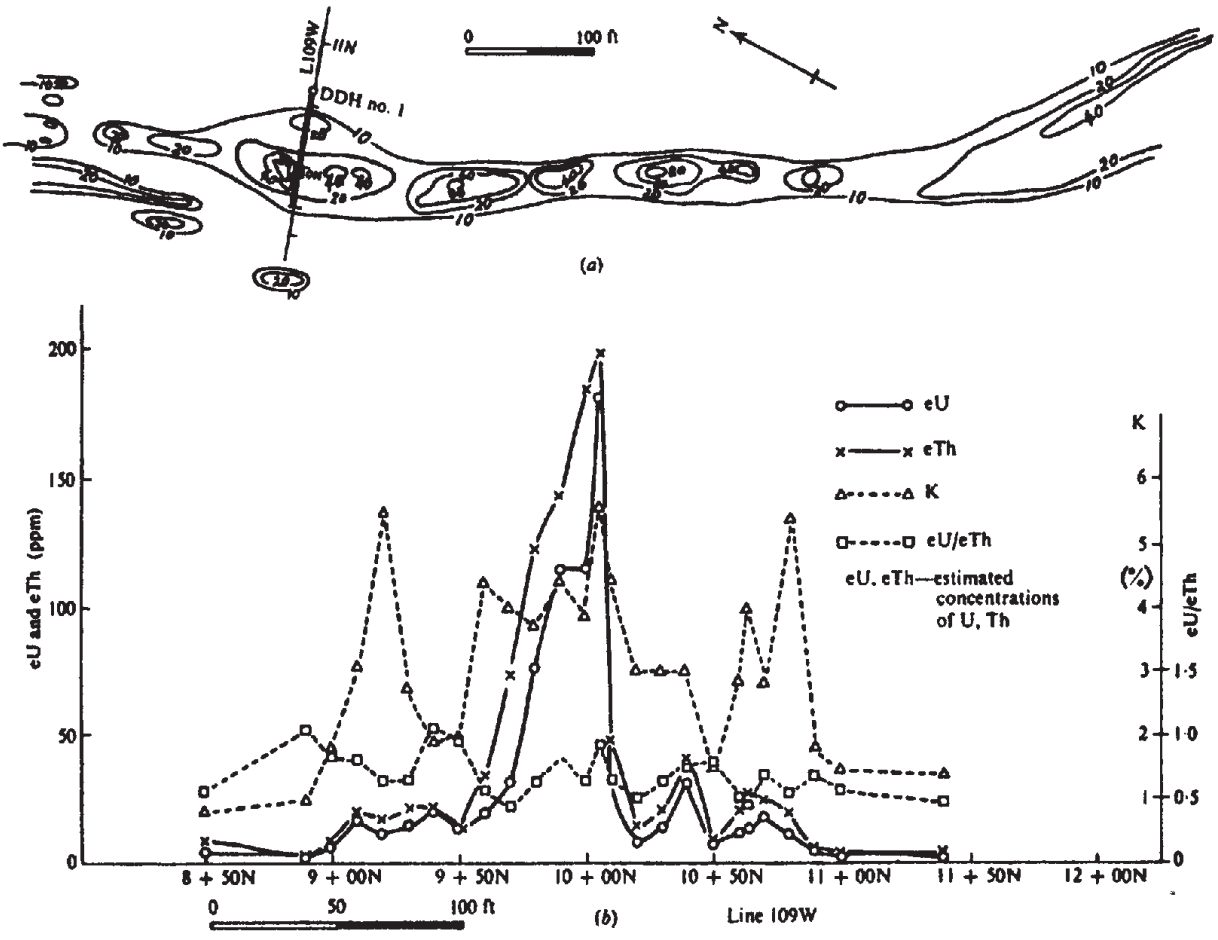

Figure 10.19. Results of radiometric survey over pegmatite, Portneuf, Quebec. (a) Isorad contours; contour interval 1,000 counts/min. (b) Radiometric profiles of eU, eTh, K, and eU/eTh ratio for line 109W.

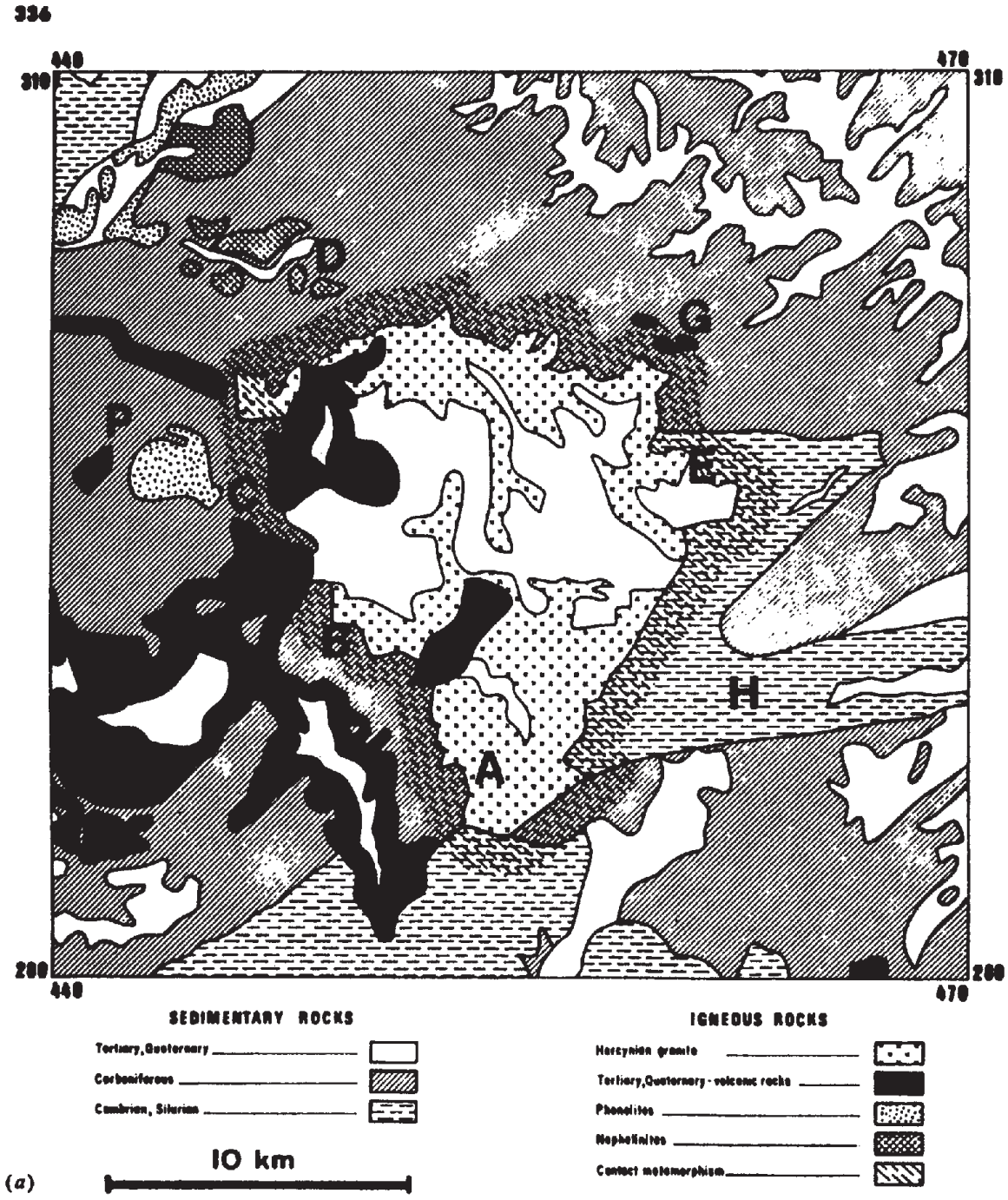

Figure 10.20. Airborne radiometric and magnetic surveys over granite zone, Morocco. (a) Detailed geology of the area.

yields the thorium count rate that would be observed at the same instant in the 1.76 MeV channel.

Theoretically only one thorium, two uranium, and three potassium standard samples are required to furnish the data to solve the three equations and determine the three constants, k_1, k_2, k_3. In practice it is best to use as many standards as possible because of instrumental and sampling errors.

The readings in Table 10.7 were obtained with a γ-ray spectrometer in a traverse perpendicular to foliation across a granite-gneiss outcrop near St. Columban, Quebec.

Given that $k_1 = 0.6$, $k_2 = 0.13$, $k_3 = 0.020$, $S_1 = 1.0$, $S_2 = 1.5$, and $S_3 = 1.7$, determine the

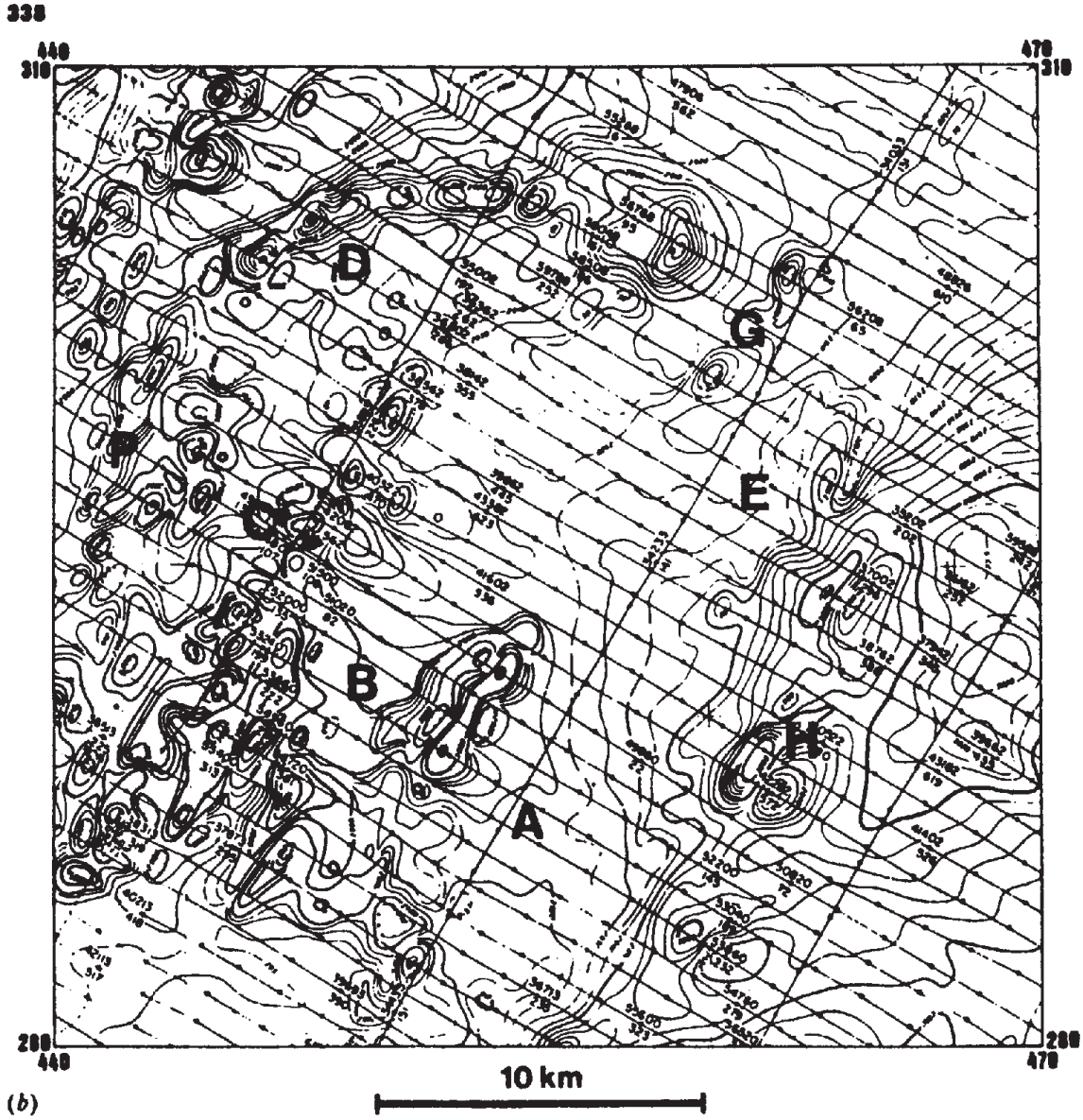

Figure 10.20. (Continued) (b) Total-field magnetic map; contour interval five gammas.

Th, U, and K content at each station and plot profiles for each element as well as a profile of the Th : U ratio.

The formation appears to be homogeneous, that is, completely granitized, except for remnants of sedimentary rocks at 35 and 215 ft. Do the profiles bear this out over the whole 500 ft traverse or any part of it? On the assumption that high Th : U ratios would be more characteristic of sediments than of the granite-gneiss intrusive, does the Th : U profile provide any additional information? Is the sampling density adequate for a petrogenic study of the rocks?

5. Figure 10.17 shows radiometric contours from an airborne test survey of Redwater oil field near Edmonton, Alberta. Figure 10.17a shows total count for γ-ray energies above 1.5 MeV, Figure 10.17b, total count only. The rocks of the area are mainly shales and sandstones, with some conglomerate, black quartzite, and argillaceous sandstone in the SW and SE corners of the survey area. Green shale forms a caprock over the oil pool.

The airborne data have been analyzed by Sikka (1959), who made corrections for variations in the radioactivity of the different soils in the area. The arithmetic mean and standard deviation were calculated for the area. The difference between each observed value and the arithmetic mean was divided by the standard deviation and the result plotted as the station value; thus, the contour interval is a multiple of the standard deviation. Sikka also measured the distribution of radon emission on the ground. In the course of this

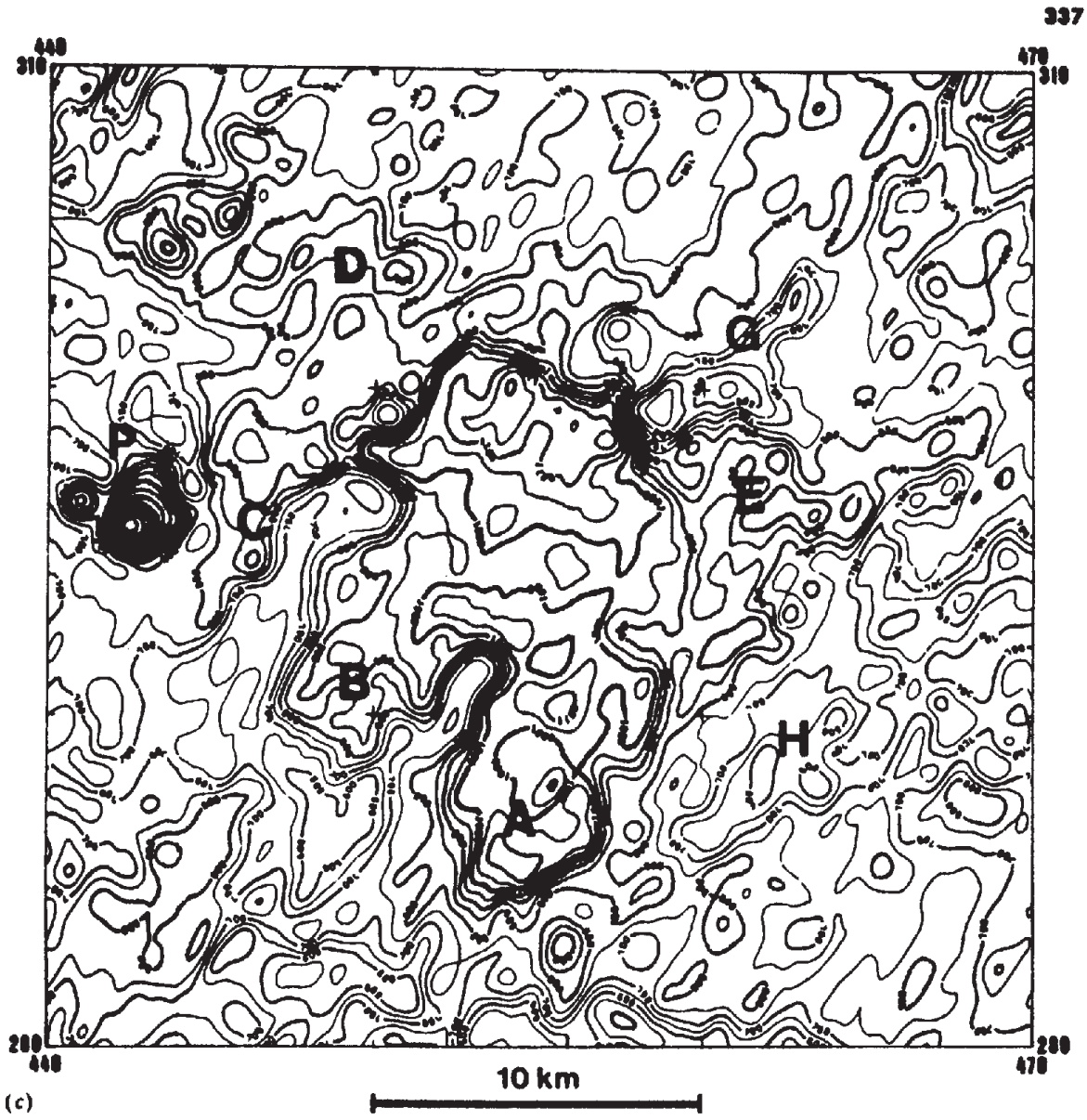

Figure 10.20. (Continued) (c) Total-count map; contour interval 50 counts/s.

work, he found that the type of soil, for example, sands, sandy loams, loams, and so forth, as well as the soil parent material, controlled the regional pattern of radioactivity to a considerable extent. Details may be found in the original work.

The airborne radiometric data from 1951 (Fig. 10.17b) were corrected only for the soil type. The contours of 1957 (Fig. 10.17a) were corrected for soil parent material as well. This was done to show the significance of both factors. Sikka states that the two maps would be similar if the complete corrections were made in both cases.

On the hypothesis that radioactivity lows reflect the relatively impervious caprock over the oil pool, try to outline its boundaries on each map. (*Note*: The survey covered only about 65% of the total area of the oilfield.) Can you spot muskeg and swamps from anomalous high radioactivity? Apart from a possible halo of high radioactivity around the oilfield, are there any structures, such as faults, indicated by linear high–low contrasts striking in a preferred direction?

6. The profiles in Figure 10.18 are taken from a detailed survey for base metals and uranium. Station readings were made every 10 ft. The magnetic–radiometric correlation is similar to that of Figure 10.14, although the geology is different and this anomaly has a strike length of 1,600 ft. Locate the radioactive source, the boundaries of the magnetic anomaly, and the dip of the mineralized section. What is the likely source of the magnetic mineralization?
7. Some results from a radiometric survey over a pegmatite in Portneuf County, about 35 miles

west of the city of Quebec, are shown in Figure 10.19. This feature outcrops continually for a distance of about 1,100 ft. As can be seen in Figure 10.19a the strike is roughly N20°W over most of the length, the main width varying between 30 and 80 ft; there are narrower pegmatitic bands on the flanks. The host rocks are gneisses with some hornblende.

The uranium, thorium, and potassium content of the rocks, shown in the profiles of Figure 10.19b, were determined with a multichannel γ-ray spectrometer by a method similar to that described in problem 4. Locate the main pegmatite section and any additional pegmatite bands with the aid of these data. Are these sections of shallow or steep dip? Can you determine the direction of dip? Does the uranium mineralization appear to be of economic grade? Compare the U : Th ratios with the actual uranium and thorium concentrations at various places along the profile. Do large ratios correlate with high uranium content?

8. The maps in Figure 10.20b and c are taken from a large-scale airborne magnetic and radiometric survey in Morocco, carried out in 1972. Geology of this 30 × 30 km granitic zone is illustrated in Figure 10.20a. Flight lines were NW–SE, with 1 km spacing at 150 m ground clearance. Data compilation was by computer, corrected for altitude; radiometric background was obtained before and after each flight by means of a short pass at 600 m, whereas a fixed magnetic ground station provided a similar check for the magnetic data. Only total count radioactivity is shown here, although Th, K, Th/K, and U counts were also available from the three-channel spectrometer.

   Make a sufficiently detailed tracing of the total count and magnetic contours for overlays on the original maps of Figure 10.20. Assess the correlation and complementary information obtained by the airborne data with respect to the geologic map; do the same for the two survey methods. Is there evidence of much overburden in the area? From the limited lists of rocks and minerals in Tables 10.4 and 10.5, can you suggest any further anomalies that might appear on the Th and K maps? Why was the U channel not reproduced?

REFERENCES

Abdoh, A. B., 1984. Field geophysical studies in the Pierrefonds-Ile Bizard region, Montreal. M.Sc. thesis, McGill Univ., Montreal.

Bates, R. G. 1966. Airborne radioactivity surveys, an aid to geologic mapping. In *Mining Geophysics*, Vol. I, pp. 67–76. Tulsa: Society of Exploration Geophysicists.

Bristow, Q. 1979. Gamma-ray spectrometric methods in uranium exploration – airborne instrumentation. In *Geophysics and geochemistry in the search for metallic ores*, P. J. Hood, ed., Econ. Geol. Report 31, Geol. Surv. Canada, pp. 135–46.

Bristow, Q., Carson, J. M., Darnley, A. G., Holroyd, M. T., and Richardson, K. A. 1977. Specifications for federal-provincial uranium reconnaissance program 1976–1980 airborne radioactivity surveys. Geol. Surv. Canada Open File No. 335.

Crossley, D. J., and Reid, A. B. 1982. Inversion of gamma-ray data for element abundances. *Geophysics* 47, 117–26.

Curry, W. H., III 1984. Evaluations of surface gamma radiation surveys for petroleum exploration in the Deep Powder River Basin, Wyoming, In *Unconventional Methods in Exploration for Petroleum and Natural Gas III*, M. J. Davidson and B. M. Gottlieb, eds. pp. 25–40. Dallas: Southern Methodist University Press.

Darnley, A. G. 1970. Airborne gamma-ray spectroscopy. *Can. Inst. Min. Bull.* 63, no. 694, 145–54.

Darnley, A. G., Cameron, E. W., and Richardson, K. A. 1975. The federal-provincial uranium reconnaissance program. In *Uranium exploration '75*, Geol. Surv. Canada Paper 75-26, pp. 49–63.

Duval, J. S. 1983. Composite color images of aerial gamma-ray spectrometric data. *Geophysics* 48, 722–35.

Gnojek, I., and Prichystal, A. 1985. A new zinc mineralization detected by airborne gamma-ray spectrometry in northern Moravia (Czechoslovakia). *Geoexplor.* 23, 491–502.

Grasty, R. L. 1979. Gamma-ray spectrometric methods in uranium exploration – theory and operating procedures. In *Geophysics and geochemistry in the search for metallic ores*, P. J. Hood, ed., Econ. Geol. Report 31, Geol. Surv. Canada, pp. 147–61.

Killeen, P. G. 1979. Gamma-ray spectrometric methods – application and interpretation. In *Geophysics and geochemistry in the search for metallic ores*, P. J. Hood, ed., Econ. Geol. Report 31, Geol. Surv. Canada, pp. 163–229.

King, C. Y. 1978. Radon emanation on San Andreas fault. *Nature* 271, 516–19.

Sikka, D. A. 1959. A radiometric survey of Redwater oilfield, Alberta, Canada. Ph.D. thesis, McGill Univ., Montreal.

Soonawala, N. M. 1968. Correlation of ground and airborne radiometrics. M.Sc. thesis, McGill Univ., Montreal.

Soonawala, N. M. 1976. Diffusion of radon 222 in overburden and its application to uranium exploration. Ph.D. thesis, McGill Univ. Montreal.

Soonawala, N. M., and Telford, W. M. 1980. Movement of radon in overburden. *Geophysics* 45, 1297–1315.

Telford, W. M. 1983. Radon mapping in the search for uranium. In *Developments in Geophysical Exploration Methods – 4*, A. A. Fitch, ed., pp. 155–94. New York: Applied Science Publishers.

Warren, R. K. 1977. Recent advances in uranium exploration with electronic alpha cups. *Geophysics* 42, 982–9.

Weart, R. C., and Heimberg, G. 1981. Exploration radiometrics postsurvey drilling results. In *Unconventional Methods in Exploration for Petroleum and Natural Gas II*, B. M. Gottlieb, ed., pp. 116–23. Dallas: Southern Methodist University Press.

Wollenberg, H. A. 1977. Radiometric methods. In *Nuclear Methods in Mineral Exploration*, J. Morse, ed., Ch. 2, pp. 5–36. Amsterdam: Elsevier.